MULTIFUNCTION SENSOR TECHNIQUE

ROLAND PITTMAN

FOREWORD

This report was prepared by Roland Pittman, Instrumentation and Control Operations, National Water Lift Company Division, Pneumo Dynamics Corporation, Grand Rapids, Michigan, under USAF Contract Nr. AF 33(615)1200. The contract was initiated under Project Nr. 8222, "Control Data Systems and Instrumentation for Advanced Military Vehicles", Task Nr. 822209, "Vehicle Body Orientation and Response Sensing Techniques". The work was administered under the direction of the Flight Control Division, Air Force Flight Dynamics Laboratory, Research and Technology Division, Air Force Systems Command, Wright-Patterson Air Force Base, Ohio, Mr. A. P. DeThomas, Project Engineer.

This is a final technical report and covers work conducted from February, 1964 to February, 1965. The manuscript was released by the author in March, 1965 for publication as an RTD Technical Report.

Principal contributors to the program were Donald R. DeMaagd, mechanical design; Robert F. Elder, electronics design; Paul R. Riemersma, mechanization; and John P. Phillips, project coordination.

This technical report has been reviewed and is approved.

W. A. Sloan, Jr.
Colonel, USAF
Chief, Flight Control Division
Air Force Flight Dynamics Laboratory

ABSTRACT

The applied research study, as described herein, relates to an investigation into the feasibility of a technique for sensing, simultaneously in two axes, angular velocity and linear acceleration in a transducer with one moving part.

Techniques for instrumenting inertial interactions in a rotating frame were employed, utilizing piezoelectric electrostrictive devices for instrumentation, and fluid bodies for the inertial reaction member and proof mass. The technique was reduced to practice, resulting in a subminiature, fully integrated, compact, functional prototype wherein both types of outputs were provided in each of two orthogonal sensing axes. An integrated prototype was evaluated for all major performance parameters and operational characteristics.

The results have revealed a transducer technique capable of angular velocity sensing thresholds of 1°/hr. and linear acceleration sensing thresholds of 10^{-5} "G", with dynamic ranges in each of the two quantities in excess of one million to one. Also demonstrated, within the study, was the potential for high reliability redundant sensing techniques and further size and power consumption reduction while maintaining the extreme sensing thresholds.

TABLE OF CONTENTS

LIST OF ILLUSTRATIONS

1. INTRODUCTION

In February of 1964, the Instrumentation and Control Operations, National Water Lift Company, under the auspices of the Air Force Flight Dynamics Laboratory, Research and Technology Division, undertook an applied research and development program to establish the feasibility of a technique for sensing two mutually perpendicular axes of angular velocity and linear acceleration in a single instrument, with only one moving part. This technique involved the use of a rotating inertial measurement frame and utilized piezoelectric devices for the sensing instrumentation.

Feasibility studies and early model work on the multifunction sensor device were performed under a company sponsored program which gave rise to the unique geometries and combinations involved in this program. The program involved the building and testing of a hydrostatic, spin axis supported, working model combining the fluid rotor rate sensor with the rotating linear accelerometer.

1.1 PROGRAM GOALS

The primary goal of this program was to establish the feasibility of a multisensor technique which, because of its geometry and construction, would imply subminiature size, minimum weight and power consumption - with much reduced complexity and increased reliability and life. In addition, goals included a multifunction aspect, namely, a two axis angular velocity and two axis linear acceleration sensing capability with performance in these areas comparable to or exceeding that of contemporary instrument types.

1.2 PRINCIPLES OF OPERATION

1.2.1 Angular Velocity Meter Portion

The angular velocity sensor is based on the unique operation of the geometry of a contained fluid body rotating at high velocities. (See Figure 1.) Examination of the series of figures denoting the instantaneous location of the inertial member at discrete 90° positions about the spin axis shows that, due to the angular momentum vector of the mass and as a result of an applied angular velocity vector at right angles to the spin axis, an error signal is generated. This error signal is sinusoidal in function and has a frequency directly corresponding to the spin axis angular velocity, with amplitude proportional to the applied input.

Manuscript released by author in March 1965 for publication as an **RTD Technical Report.**

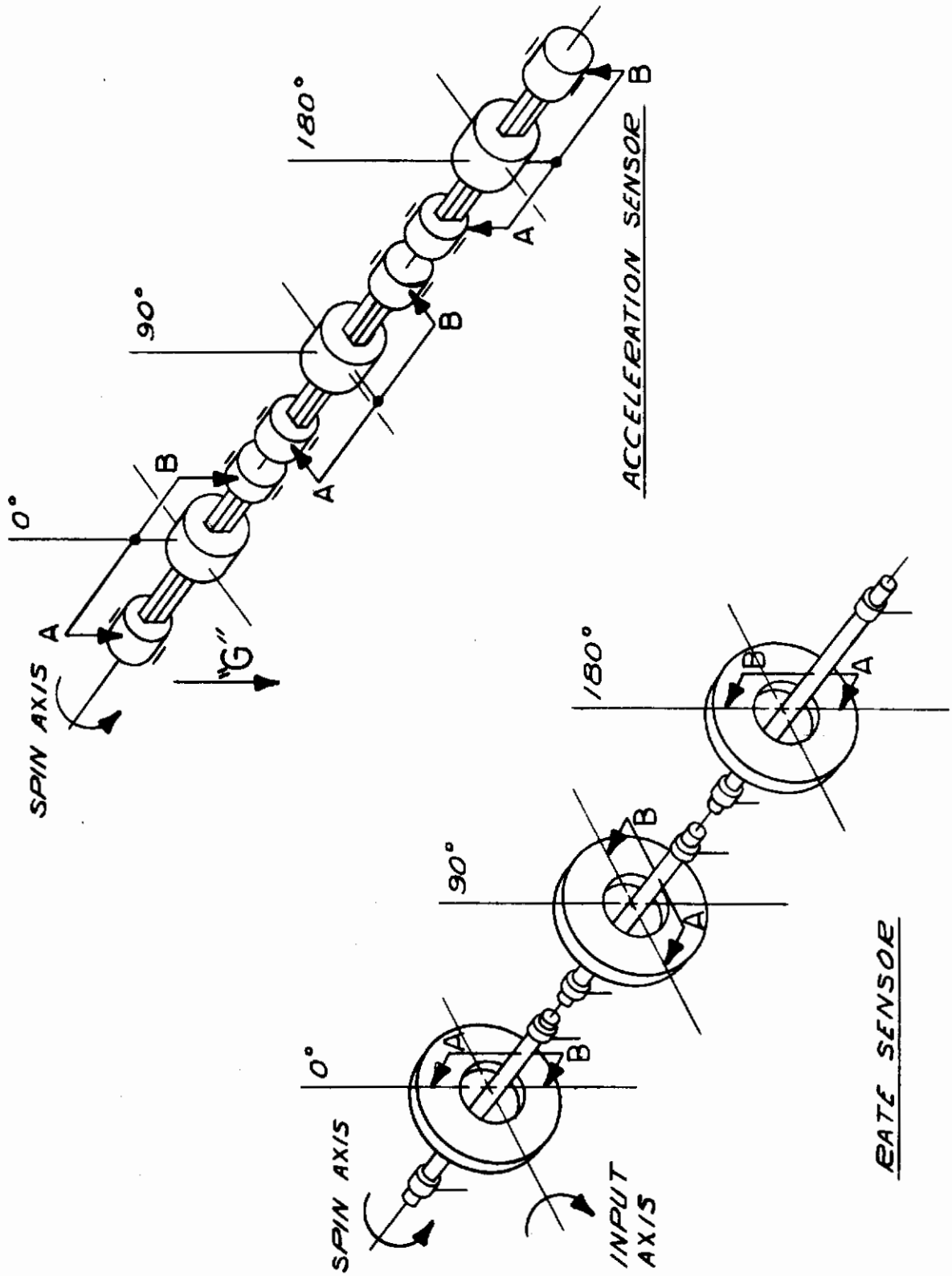

Figure 1. Principles of Operation

It is to be noted that this geometry operates in such a manner as to modulate a D.C. input. Hence, there is no need for an electrical carrier excitation for the pickoff to operate. This leads to important considerations for the attainment of very low thresholds due to the absence of null quadrature and other pickoff limitations. Major limits imposed on the threshold of this device are in the quality of the spin axis bearing technique.

To examine the instrument for sources of error comparable to similar sensing devices, whereas most conventional transducers suffer from sources of D.C. torque disturbances, this device does not respond to static, but rather dynamic disturbances. In other words, torques which have components in phase and in synchronism with the rotating member can yield the equivalent of a bias. Further, these vibrations have to be uniquely oriented with respect to the spinning axes; for instance, a pulsing torque vector which is at once at right angles to the spin axis and also the sensitive axis of the crystal geometry.

To note the effects of a linear "G" field on the rate sensor, consider that the pickoff operates in essentially a velocity mode and, as such, does not have a voltage which is a measure of a unique geometric position, but one which is proportional to the total amplitude at which it is bent. The presence of steady-state deflections on the crystal give no output. Further, due to the unique dipole geometry of the pickoff, common mode rejection operates for all linear disturbances. For vibrations along the spin axis which act on the unfloated mass of the pickoff crystal assembly, the symmetry of the dipole arrangement operates to give a 10 to 100 times reduction in transferred noise. In addition, this geomtery does not exhibit an anisoelastic term in its operation due to the inability of the fluid to transmit radial torques.

1.2.2 Linear Acceleration Portion

The utilization of crystal sensing devices in a rotating frame to instrument linear acceleration involves a proof mass rotating on a contactless bearing with crystals mounted in series with the radial load-carrying train (see Figure 1). Here, the pickoff members are monolithic bender crystals with an extremely high gage factor working as structural supports to the proof mass and operating as follows:

If two crystals are arranged in a dipole to radially support a mass, each crystal goes from a compressive to a tensive mode once every revolution at the carrier frequency. This generates a voltage with a frequency identical to the spin frequency and with an amplitude proportional to the stress amplitude.

The two principal data formats for resolving and demodulating the multifunction sensor two axis information are depicted in Figure 2.

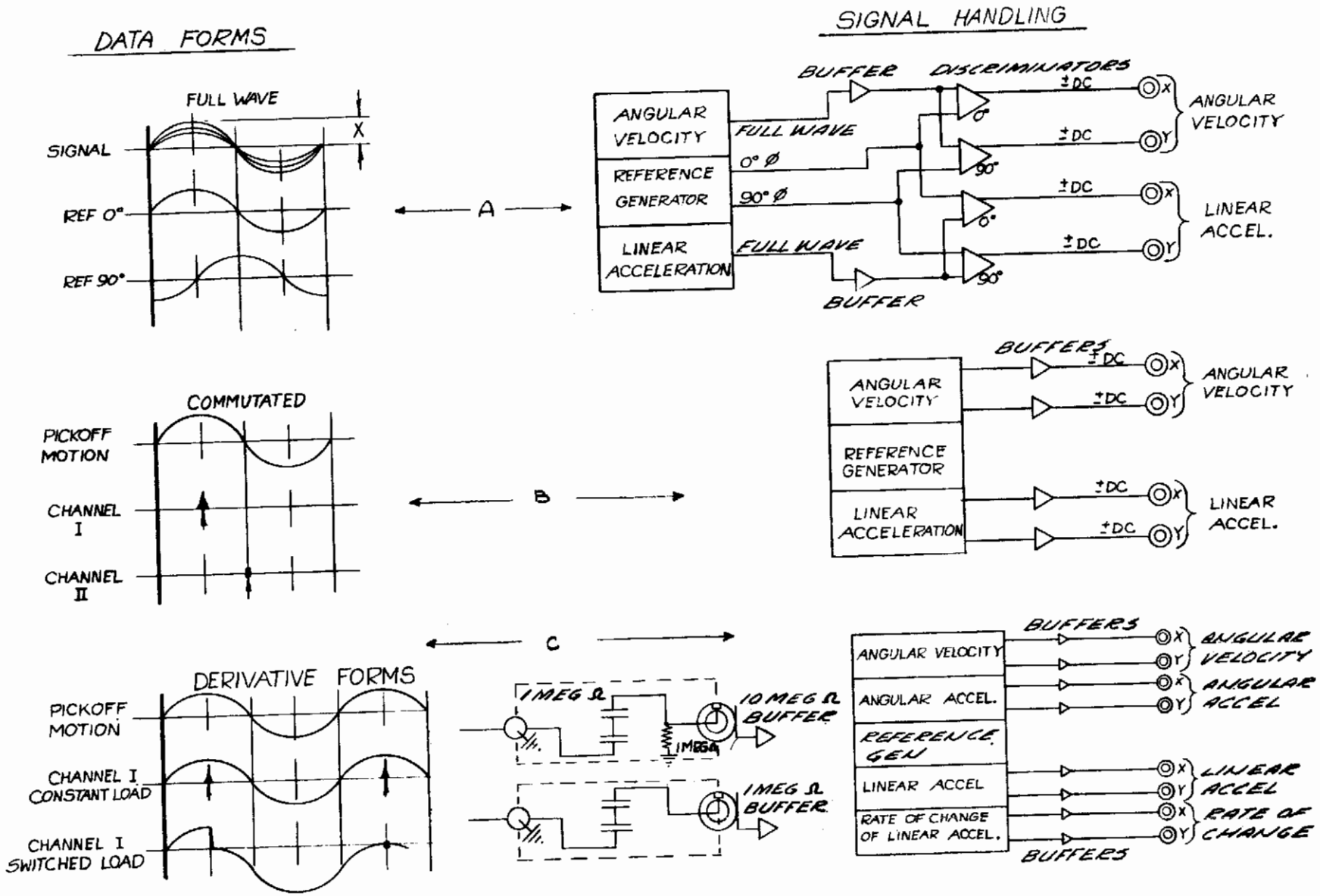

Figure 2. Multifunction Sensor Output Data Format and Signal Handling

2. DESIGN AND EVALUATION OF MAJOR COMPONENTS

2.1 OVERALL DESIGN - MULTIFUNCTION SENSOR

The design of the prototype multifunction sensor is depicted in Figure 3 showing the details for the hydrodynamic bearing, spin motor and reference generator. It should be noted that the sensing element, which includes the rate sensing cell and the accelerometer pickoff, form a complete hermetically sealed chamber suitable for directly mounting into the gas bearing journal. The test and evaluation approach used was to design and fabricate a combined sensing cell, as shown, to be preliminarily tested in a ball bearing configuration before installing it in the gas bearing, thus allowing simultaneous development of the bearing motor combination and of the cell.

2.2 ACCELEROMETER PICKOFF

2.2.1 Rectilinear Vibration Tests

A series of tests were run on several crystal coupling geometries to arrive at an optimum crystal arrangement in terms of scale factor, isolation from unwanted inputs (both rotational and rectilinear), and compact, simple arrangement.

The resulting design, as shown in Figure 4, consists of four compressor crystals on each end of the proof mass arranged in a radial fashion. In order to allow high order compliance in all directions except the compression mode, a welded pivotal joint was used. As shown in Figure 5, the performance of this geometry in terms of cross coupling, isolation and scale factor, as evaluated on a rectilinear shaker table, was very good.

Plot 1 of Figure 5 depicts the output for the primary sensing mode at a one "G" level over a frequency range of 100 to 4,000 cps. This arrangement very closely approximates the crystals' dynamic situation as it later occurred in the rotating geometry at a specified carrier frequency. It is important to note that, for the Q's and masses involved, which closely simulate the actual multifunction sensor, the scale factor is linearly decreasing with frequencies from 50 to 2,000 cps with a nominal output in the order of 125 millivolts per "G" at the 400 cps point. The difference between the 200 and 400 cps carrier resulted in only a 10% gain change. This was a fortunate situation in that it allowed a reasonable spin frequency range without undue scale factor attenuation.

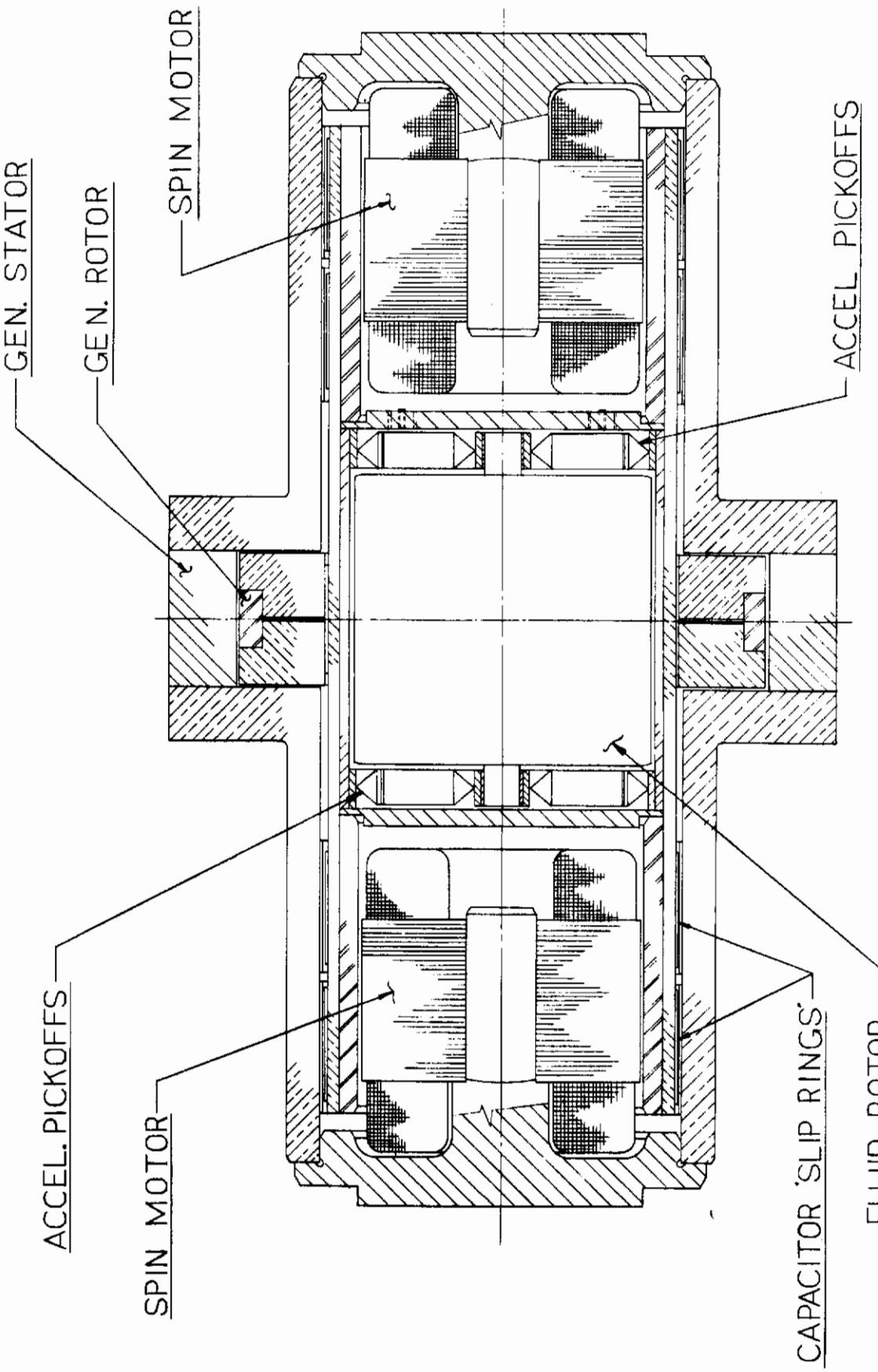

Figure 3. Multifunction Sensor Layout Drawing

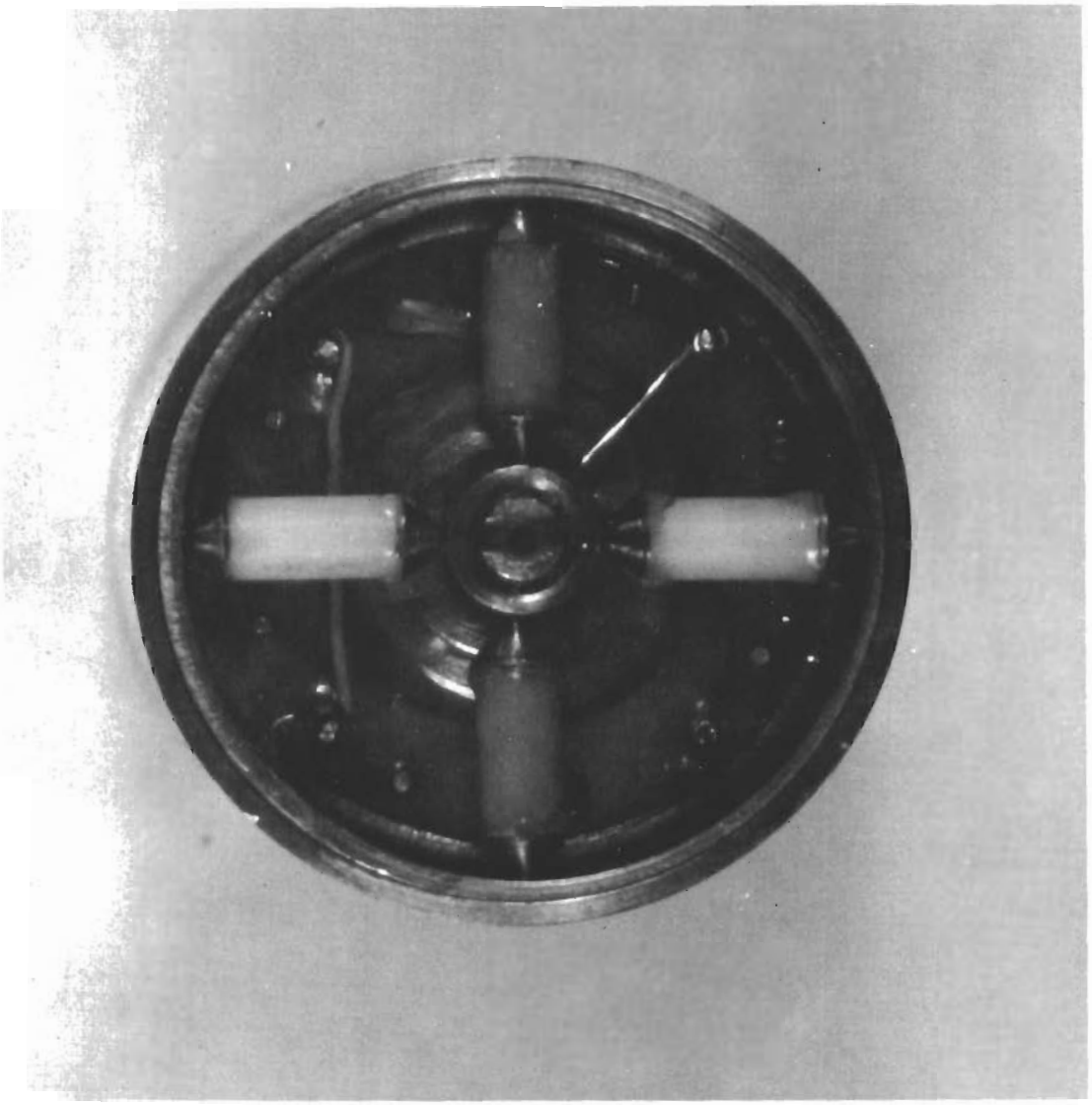

Figure 4. Accelerometer Pickoff Compressor Crystal Arrangement

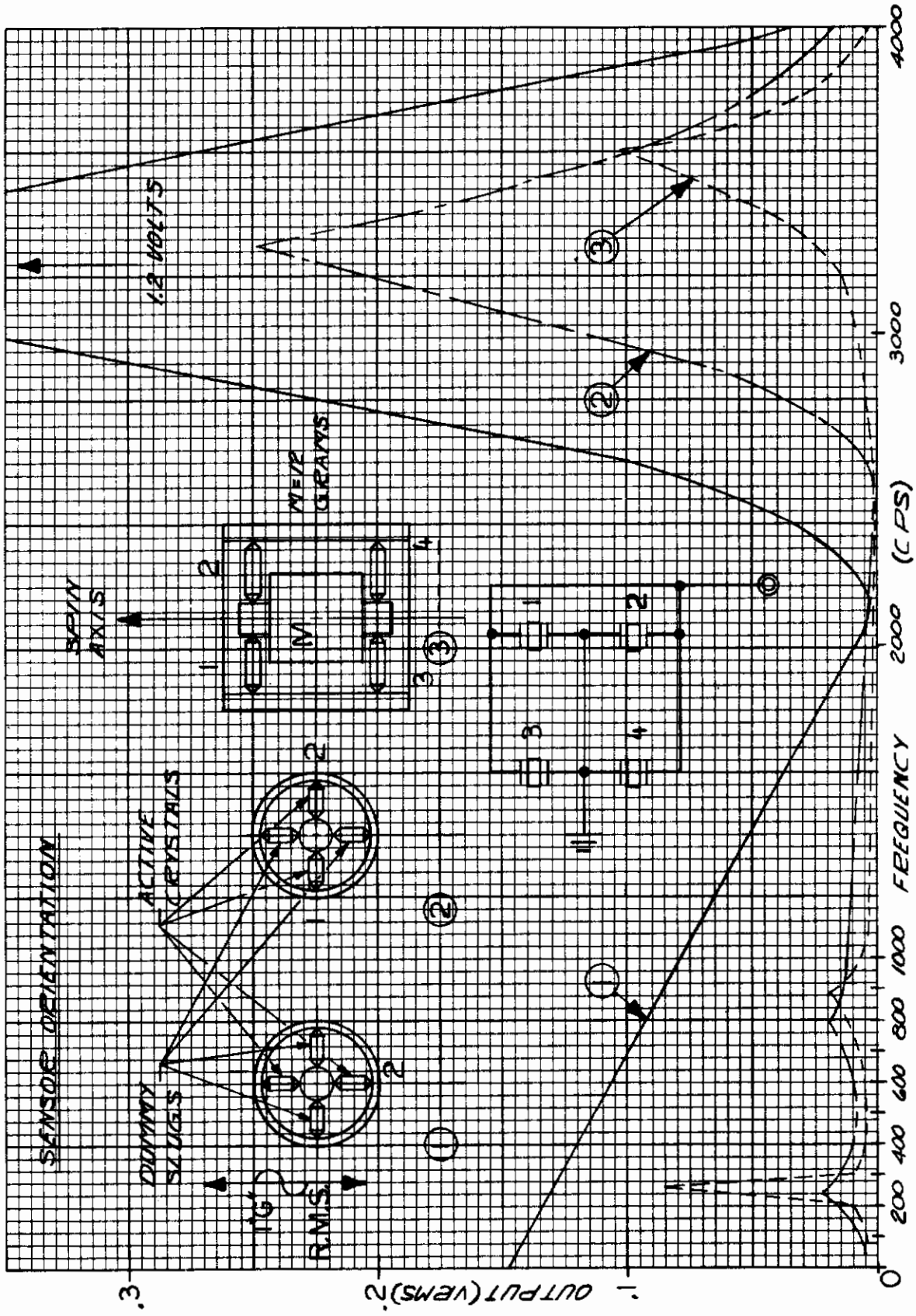

Figure 5. Accelerometer Pickoff Characteristics with Vibratory Inputs

Referring to Plot 3 of Figure 5, note the relatively flat output except at the 250 cps point which was chosen as the cut-off frequency for the mechanical filter in the rate sensor element. Two such assemblies are arranged, one on each end of the fluid rate sensing cell thereby forming a radially stiff support system for the rate input torques (see Figure 6). At the same time the accelerometer pickoff system, which is similar to a diaphragm in its axial to radial stiffness distribution, provides a compliant member along the longitudinal axis. This distribution of spring rates acts as a mechanical filter for the rate sensor to cut off rectilinear vibration directed along the spin axis, originating from outside environments. This mechanical filter is tuned to a resonant frequency of 250 cps, deliberately below the 400 cps spin carrier frequency. The reason for desiring a filter tuned at such a frequency compared to the spin frequency is to attenuate the vibrations acting on the rate sensor at identically the spin frequency, the undesirable effect of which is to cause relatively large modulations of the rate sensor output.

Referring to Plot 2 of Figure 5, the output is down until the resonant point is reached at 3,200 cps, at which point the output shows the same peaking point as Plot 1, but with a resultant attenuation due to the input direction. Based on these measurements, it was predicted that (a) the scale factor of the accelerometer system, which included four crystals in a parallel hookup with a simulated fluid rotor mass, would have an output of 300 millivolts per "G" at 400 cps carrier and would, in general, exhibit the carrier frequency sensitivity as above described, (b) a resonant frequency would be exhibited in the sensing plane of 3 to 4 KC, and a value of under 250 cps along the longitudinal axis.

2.2.2 Ball Bearing Suspension System Tests

As a preliminary step leading to the eventual inclusion of the accelerometer pickoff into a gas bearing suspension system, a ball bearing system test bed was fabricated. See Figure 7.

Referring to Figure 8, the ball bearing suspended accelerometer test bed with a solid proof mass simulating the rate sensing cell exhibited performance characteristics as predicted except for the scale factor, which was 350 millivolts per "G". In addition, the accelerometer showed the following characteristics:

Rate Sensitivity:	.0005 - .0015 V/degree/sec., or .0025 "G"/degree/sec.
Null:	Short term uncertainty (seconds to minutes) - .0037 "G"
	Long term uncertainty (minutes to hours) - .007 "G"
Threshold:	10^{-3} "G"

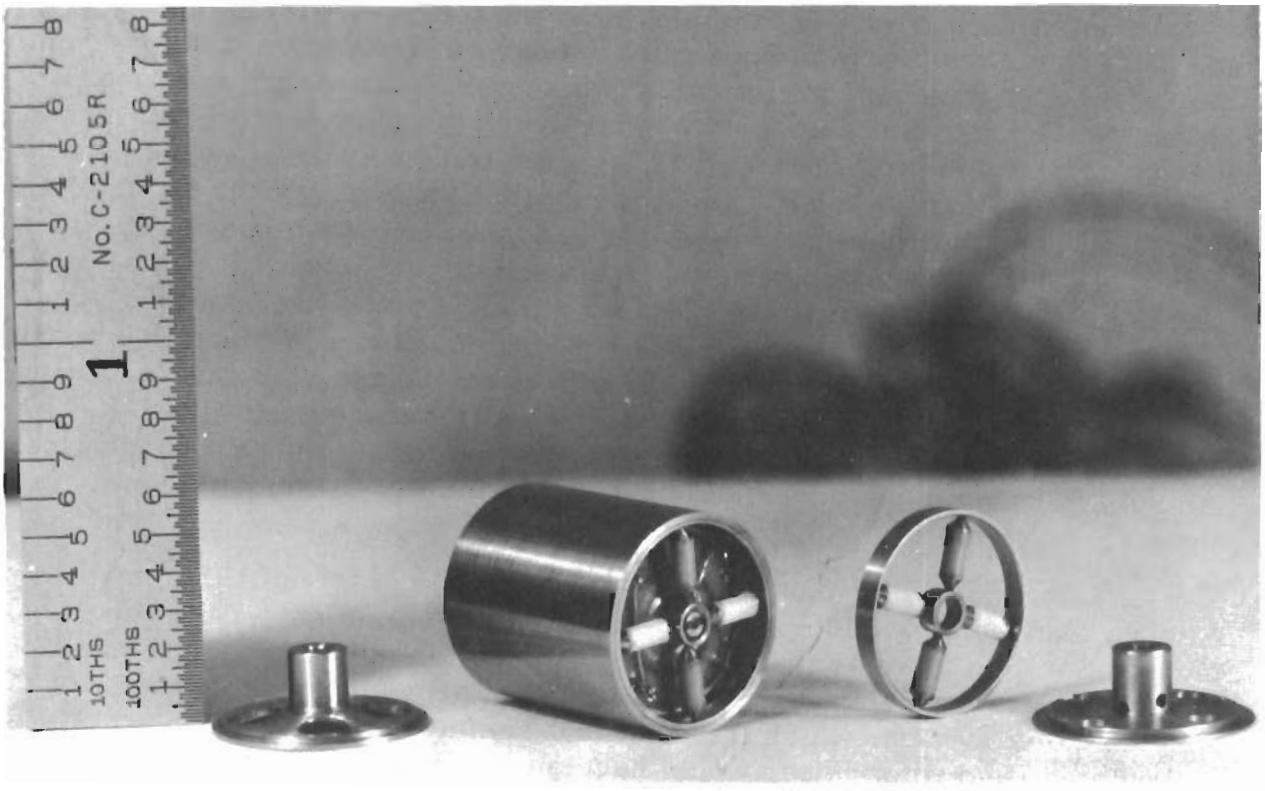

Figure 6. Accelerometer Pickoff Assembled with Angular Rate Sensing Cell

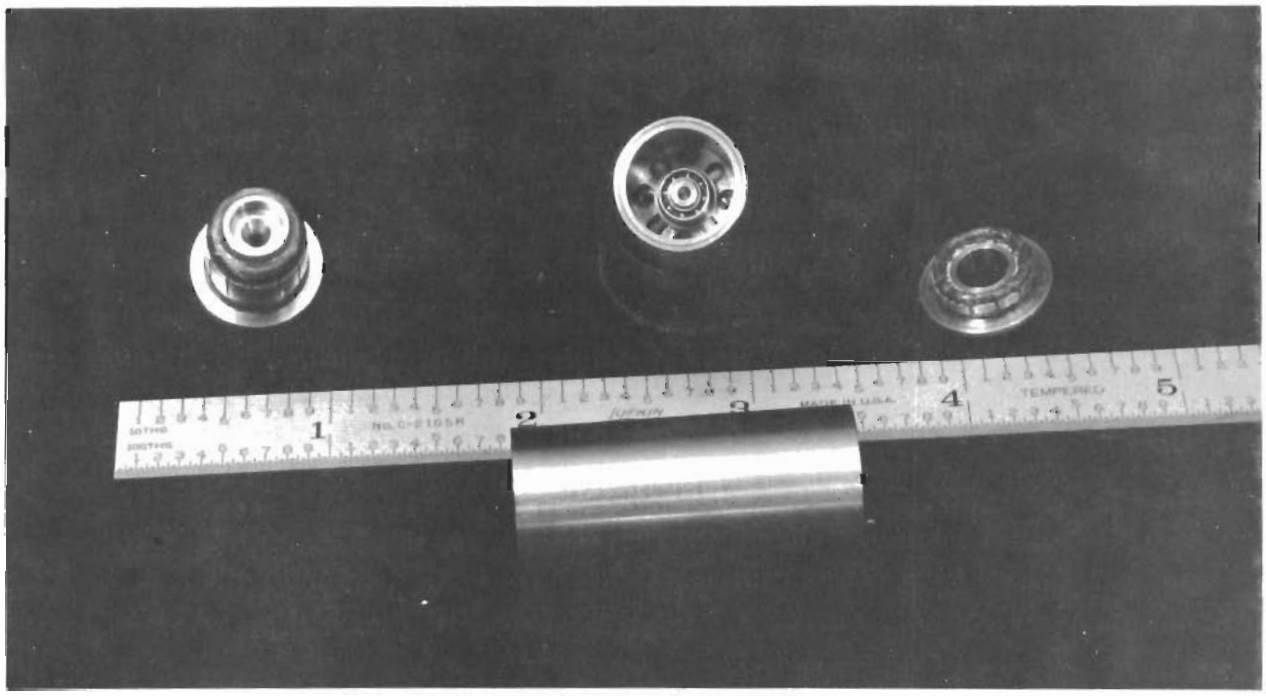

Figure 7. Ball Bearing Suspension System Test Bed

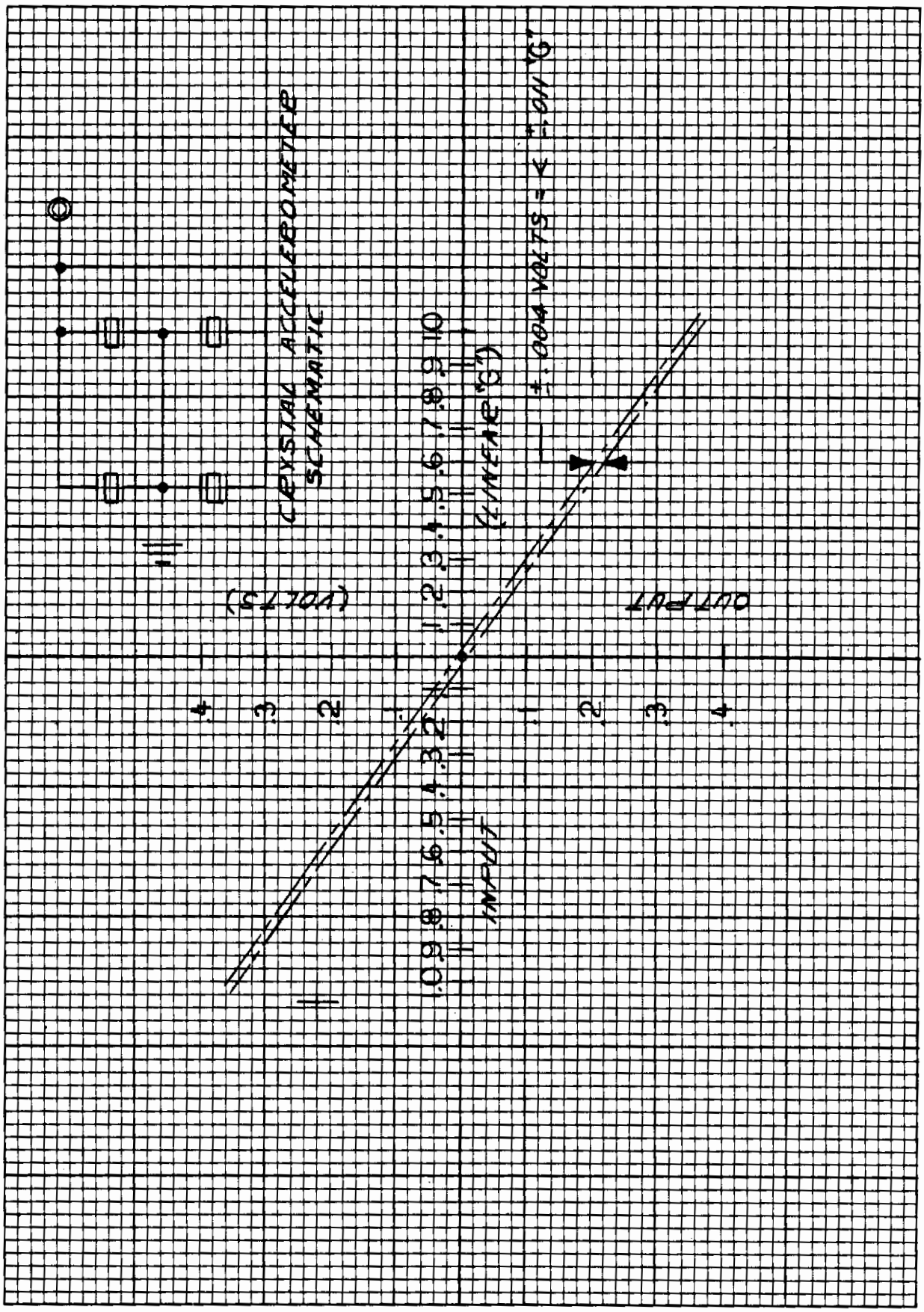

Figure 8. Accelerometer Performance in a Ball Bearing Suspension System

During this evaluation, an effect having to do with a variance in the null bias was found. It appeared to be dependent on the relative positions of the rotating magnetic vector produced by the motor winding and the rotor structure locked to it. Because the rotor comes into sync with the rotating vector in a random fashion, various members on the rotating body are subjected to a random exposure of both electromagnetic and electrostatic pickup due to imperfect shielding. This caused a ±.025 V variation in null level dependent on lock-in position. This variance was demonstrated by forcing the lock-in position to move slowly through 360°, while the corresponding null level could be seen to vary by ±.025V.

Two steps were taken to minimize this effect. The first was the use of shielding wherever possible to prevent the obvious problems due to direct coupling. Second, to be rid of the randomness due to lock-in position, a method for causing the rotor to sync repeatedly in the same relative position was incorporated. This was accomplished by the use of a ring-shaped permanent magnet placed adjacent to the normal hysteresis rotor of the synchronous drive motor (see Figure 9). The permanent magnet induces a set of permanent poles in the hysteresis element which do not adversely affect its operation during the run-up period. As the rotor approaches sync speed, the permanent poles become dominant, since the relative speed between the rotating vector and the rotor is diminishing, causing the rotating vector to lock onto the induced poles.

The above arrangement was tested, and was found to be successful in holding the motor sync position repeatability to within $<30^{\circ}$. This meant that for units where the discriminator elements were nearby, and where the lead shielding between the buffer amplifier and the discriminator inputs was controlled, the effect of the motor sync position could be controlled effectively.

In addition, the voltage necessary to hold the motor in sync was reduced considerably. Reducing the normal driving voltage of 26 V AC to about 20 V AC caused drop out of most non-modified motors. Those with the permanent magnet included remained in sync down to 10 V AC.

2.2.3 Gas Bearing Suspension System Tests

As the program and overall design of the multifunction sensor progressed, the accelerometer was combined with the rate sensing cell and tested in a hydrodynamic gas bearing suspension system.

The following summary of these results, as extracted from overall evaluation data, showed the accelerometer performance to be greatly improved.

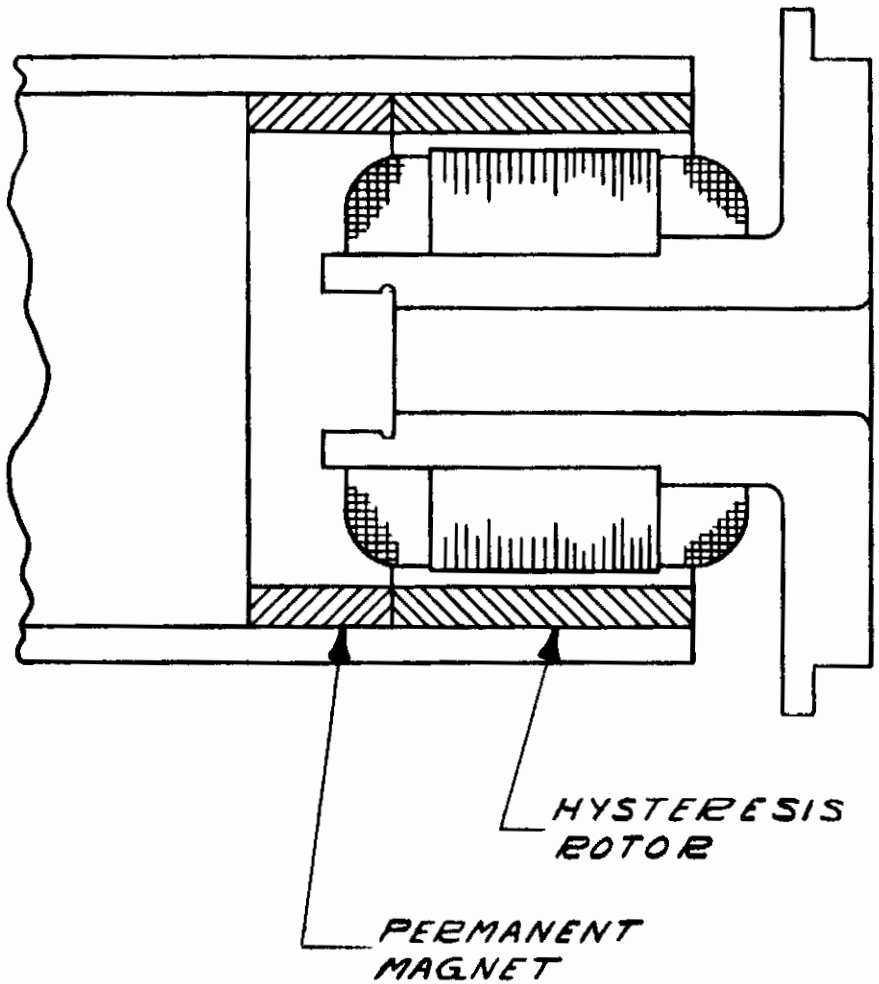

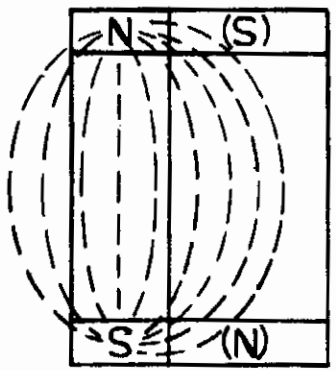

N-S - PERMANENT POLES
(N)-(S) - INDUCED POLES

Figure 9. Permanent Magnet Assembly for Motor Sync Position Repeatability

With the unit operating at 12,000 RPM, which was the speed selected as the optimum operating speed of the rate sensor, including considerations for the spin motor power consumption, the accelerometer portion was examined in detail in the one "G" field.

In five hour recorded tests, the unit exhibited a threshold of <.00005 "G" with a short term null uncertainty of <.0002 "G". The motor sync position effect on the null amounted to <.0001 "G" per 10° motor position change. The angular velocity cross coupling amounted to <.001 "G"/deg./sec. The null settling repeatibility after overrates and one "G" applied fields was very repetitive and always <±.0001 "G". The incoherent noise width band was in the order of .0005 "G's" peak to peak, becoming from time to time noisier or quieter as the ambient background noise changed. The unit exhibited changes of <.0001 "G" for ± 20% change in motor excitation flux.

2.2.3.1 Linearity

An initial measurement of the linearity of the output in the one "G" field, using ± 1% readout equipment, showed the linearity to be within this ± 1% range. These results are shown in Figure 10.

2.3 FLUID ROTOR RATE SENSING CELL

2.3.1 Ball Bearing Suspension System Tests

Although the rate sensing portion of the multifunction sensing cell had been previously developed, and partially evaluated in a ball bearing suspension system, further testing in this area was felt to be necessary to provide data as a comparison with gas bearing suspended performance. In addition, a test series on the ball bearing sensor allowed a preliminary equipment checkout and finalization without unduly jeopardizing a new instrument.

Figures 11 and 12 depict the test setup employed to achieve the following test results:

Threshold	=	<.5°/hr.
Long term null uncertainty (hour to hour)	=	<±3°/hr.
Short term null uncertainty (minute to minute)	=	<±1°/hr.

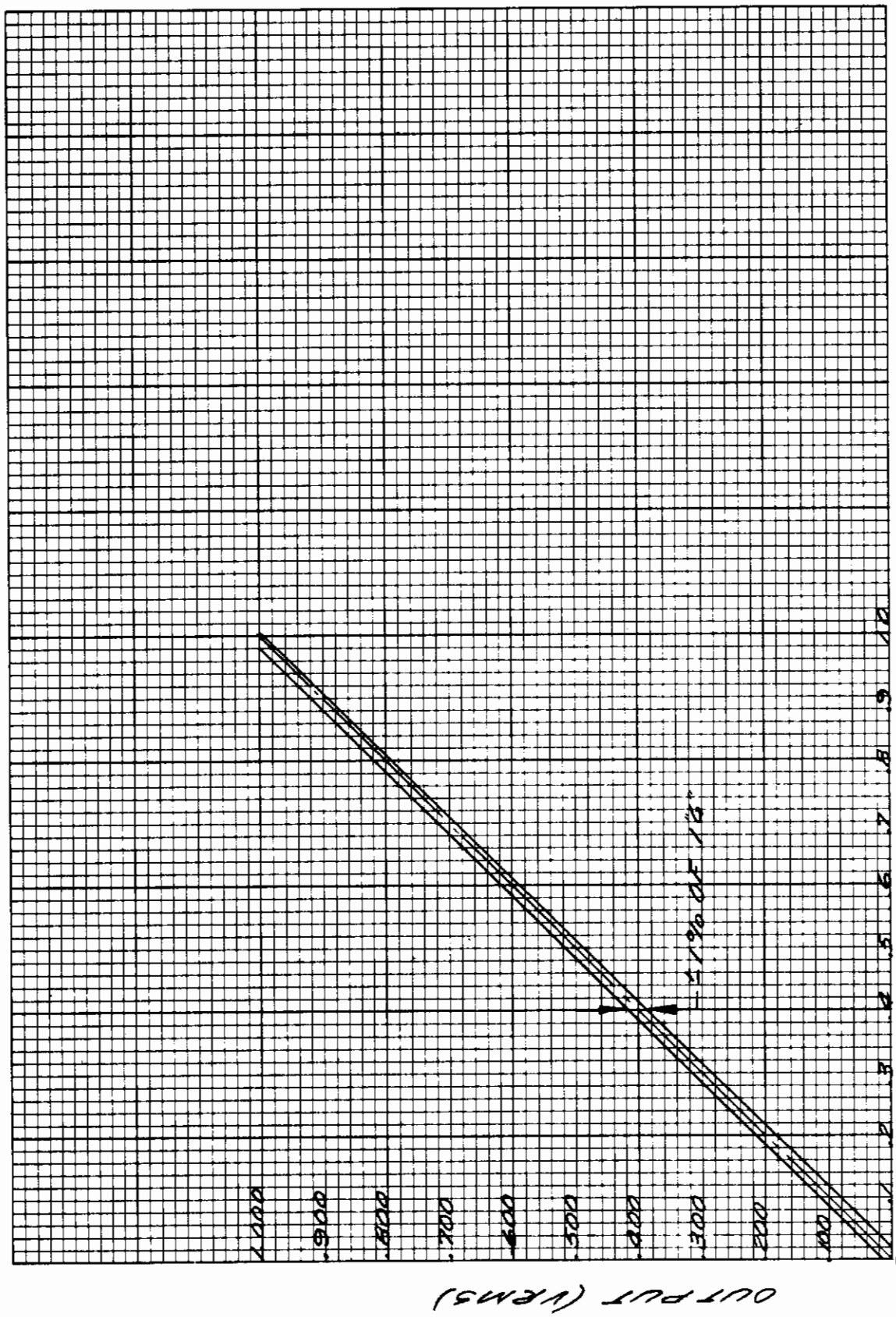

Figure 10. Accelerometer Linearity

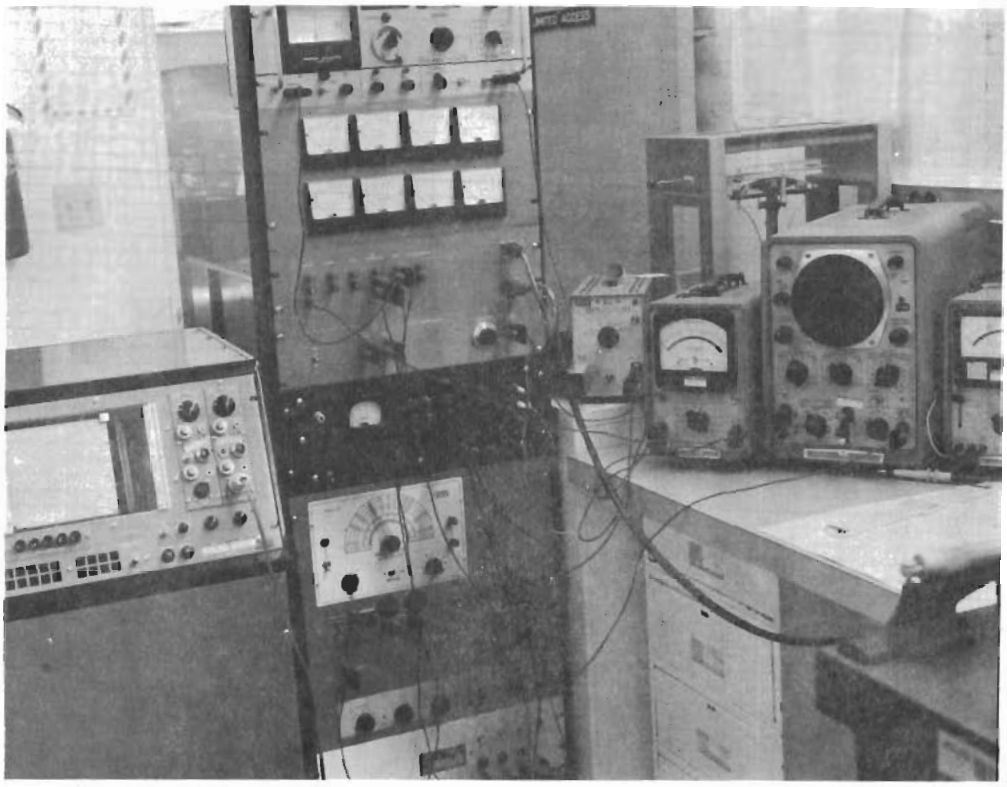

Figure 11. Test Instrumentation Console

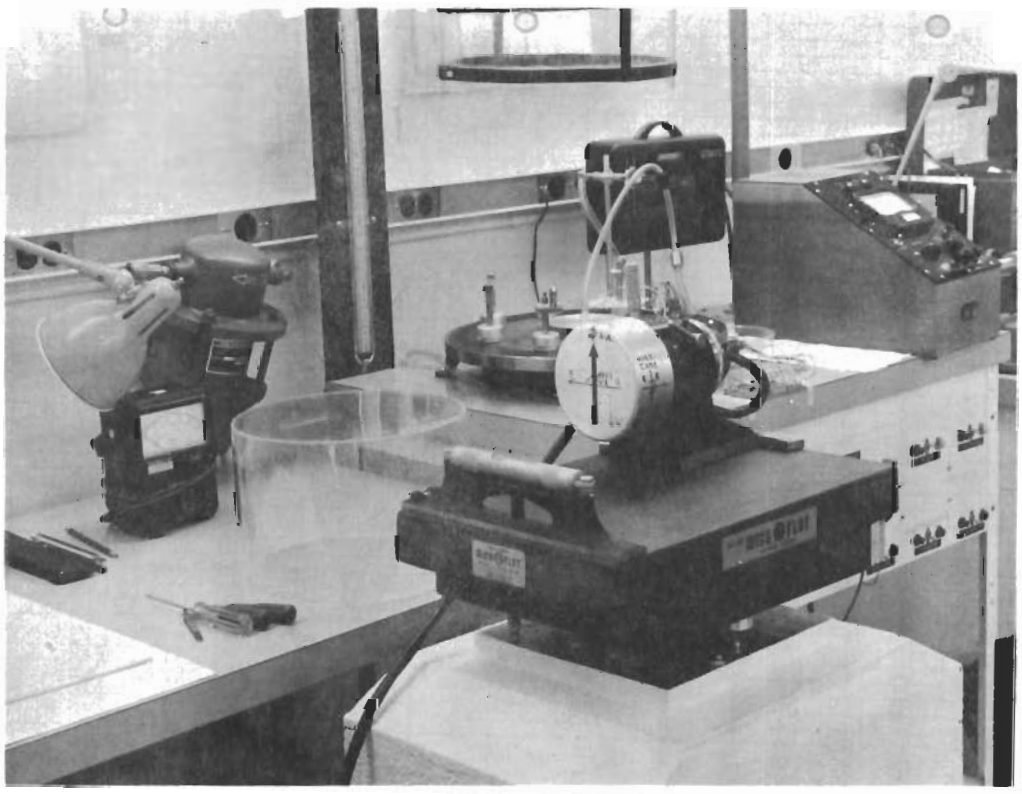

Figure 12. Transducer Measurement Pedestal and Plunging Head

Starting warm-up	=	$< 5^\circ$/hr. for total change with a repeatability at the end of 2 minutes of $< \pm 1\text{-}1/2^\circ$/hr.
Motor sync effect	=	$< 4^\circ$/hr./10° of motor sync position.
Effect of motor excitation level	=	$< 1^\circ$/hr. for 15% changes in magnitude.

(This effect attributable to the slight motor sync position change due to flux level change.)

After overrate repeatability - throughout the series of tests, 10°/hr. input was applied from time to time to check the sensitivity of the recorder setup. The inputs were introduced by turning the rate sensor about the vertical axis to couple in the horizontal earth rate component, and during this time additional overrates in excess of 100°/sec. were applied about a perpendicular axis. An inspection of the test recording immediately before and after the disturbance gave some measure of the physical repeatability of the sensor element. This repeatability in all observed cases was $< \pm .3^\circ$/hr.

2.3.2 Gas Bearing Suspension System Tests

2.3.2.1 Threshold and Null Uncertainty

After the rate sensing cell and the accelerometer pickoff were combined, as shown previously in Figure 6, they were assembled into the gas bearing.

The test data obtained on the rate sensing portion of the resulting multifunction sensor indicated that the transferred noise was reduced as the spin velocity increased over the range of from 8,000 to 14,000 RPM.

The overrate repeatability was within the resolution of the recorded data, which was $< .6^\circ$/hr.

The motor sync position effect was in the order of 2°/hr./10° motor position change.

The null stability from hour to hour was $< \pm 2^\circ$/hr.

Based on the overall rate sensor operation, it was concluded that all factors having to do with threshold uncertainty, excepting motor sync effect, would be improved at relatively high operating spin velocity. See Figure 13.

2.3.2.2 "G" Sensitive Term

Tumbling tests in a one "G" field had disclosed a significant linear "G" sensitivity term in the rate sensor. In an effort to understand and control this term, a compilation of all of the prior history with respect to the performance of this one parameter was obtained from 22 samples. The average value was found to be in the order of .02°/sec./"G", with excursions as great as .1°/sec./"G" and as small as .005°/sec./"G".

Concurrent with this, in another program, a block of three ball bearing instruments were fabricated under closely controlled conditions. The build cycle was monitored with respect to certain physical constants having to do with this problem in the normal design. This was done in an effort to see what the dispersion would be against the norm. The first unit of this group had a linear "G" sensitive term of .005°/sec./"G", which was an order of magnitude better than the average performance level of previous units.

Based on the results of an exhaustive test program involving several units with four discretely different sensor designs, and correlating the results of the data against performances of the present multifunction rate sensor pick-off geometry, the following conclusions can be made:

a) The linear "G" sensitive term is developed directly within the fluid sensing geometry proper and, as a first order effect, is not directly affected by the quality or stiffness of the spin axis suspension. In other words, it is in the rate sensing cell proper.

b) The effect is generated within the sensing cell in the following fashion. For a condition of relatively high spin velocity the fluid member begins to operate more and more as a quasi-solid and thereby able to transmit torques. This has been established by input - output versus spin velocity tests while observing the response of the coupled axis. These observed results indicated that in the range from 50 cps to 800 cps, a transition takes place at approximately 150 cps and higher wherein the fluid response to an angular input changes from "hang off" about an axis coincident with that of the input axis to a precession about a 90° axis. Therefore, under the conditions of a 200 to 400 cps carrier, the fluid member operates as a precessing torque transferring member. If for any reason this fluid body is unsymmetrical along the spin axis, it is in effect pendulous and susceptible to orientation, or "G" forces.

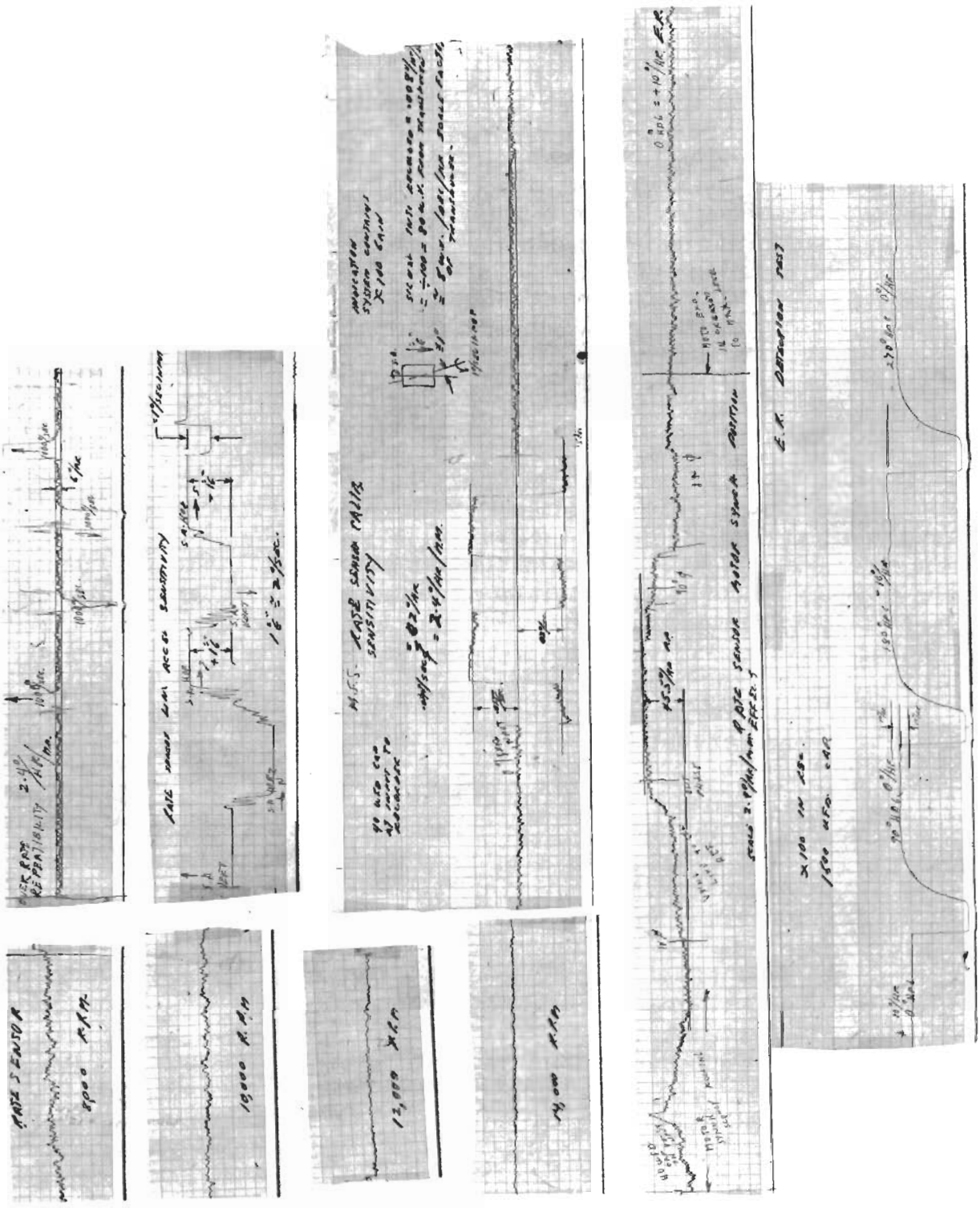

Figure 13. Threshold and Null Uncertainty Recorded Data

2.4 HYDRODYNAMIC GAS BEARING

2.4.1 Test Bed

The initial work on the gas bearing involved the fabrication and initial evaluation of a test bed. Photographs of some of the parts fabricated early in the program are shown in Figure 14 and 15, and a test setup is shown in Figure 16.

In these initial tests the spin body had not yet been dynamically balanced, which limited the top speed to less than 10,000 RPM. These initial results indicated a total RMS null in the rate sensor of less than 3 millivolts with the resolved and discriminated component being less than 60 microvolts.

2.4.2 Prototype Gas Bearing Assembly

Referring to the multifunction sensor gas bearing layout, Figure 3, and a photograph of the actual parts, Figure 17, a technique was developed for assembling all of the critical alignment joints which involved no precision tooling or alignment fixtures, and relied on the accuracy of the parts themselves as the determining factor. The technique was one where an externally coupled gas drive operated the bearing with the centering mechanism derived from the hydrodynamic properties, with a resilient adhesive applied to certain joints for fastening. The assembly was done in three stages.

a) The rotor and pumping plate were assembled to become a permanent assembly.

b) The one end frame and the outer adapter sleeve with the generator stator spacer became a permanent subassembly. At this stage the opposite end frame was introduced but not secured, with the bearing assembly being set up in the gas driven running fixture and a dead weight applied to the loose end frame for loading against the spacer. The assembly was "run in" for 40 to 80 hours, the purpose of which was to act as a micro, self-deburring operation.

c) Subsequent to this, the unit was disassembled and the major subassemblies cleaned and then reassembled with the final glue joint made using the same test assembly fixture. This procedure resulted in an extremely smooth running bearing which was very easy to fabricate and assemble.

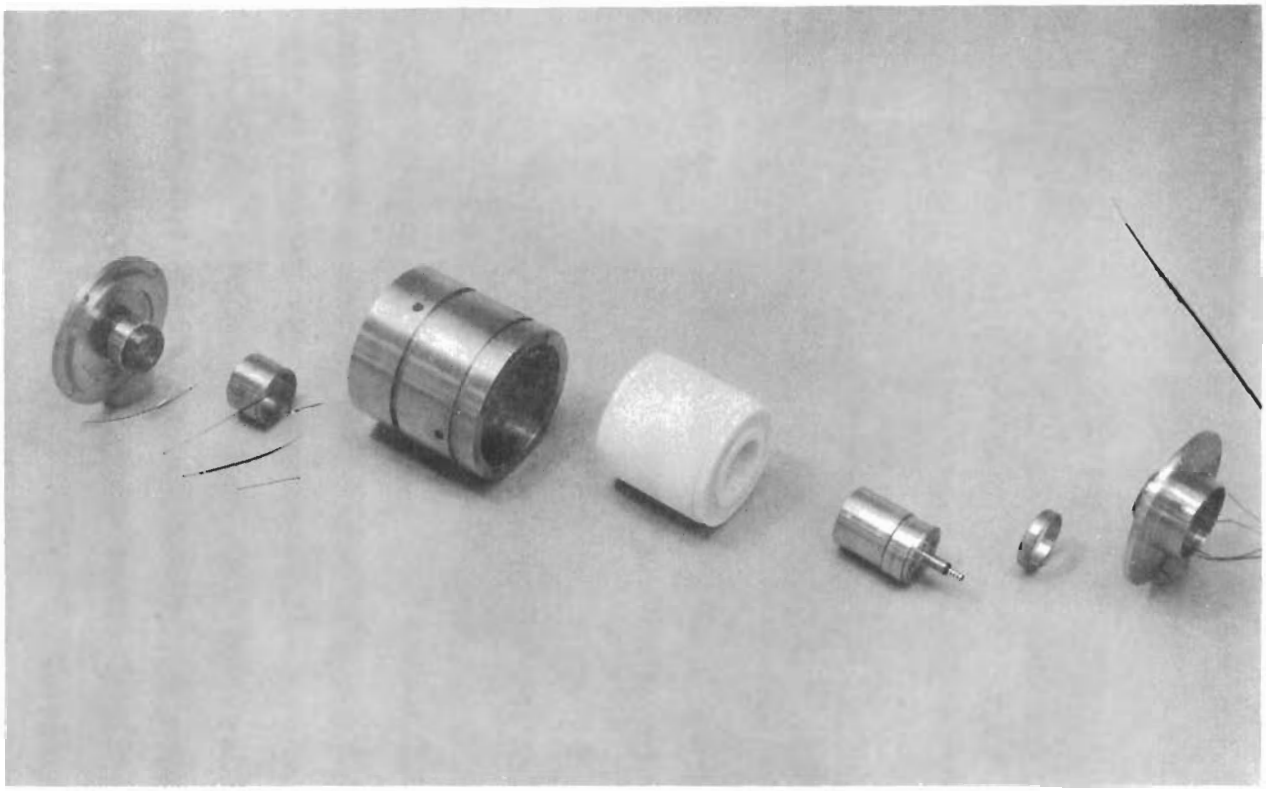

Figure 14. Hydrodynamic Gas Bearing Initial Test Bed Parts

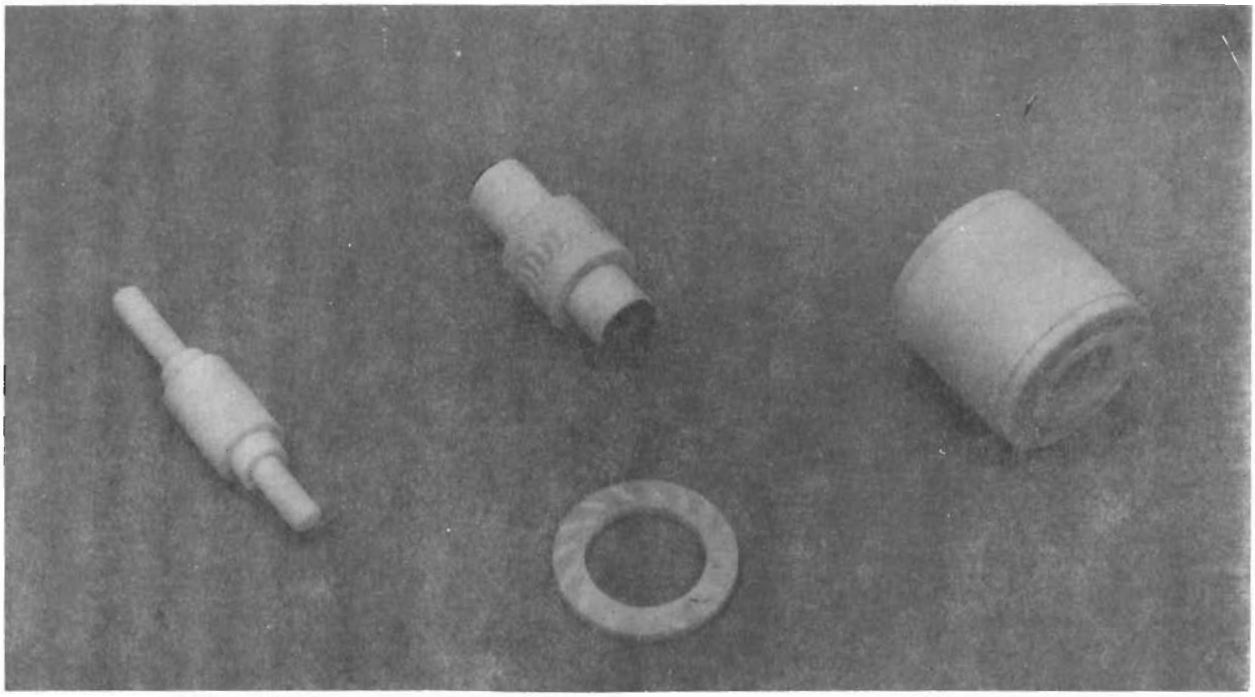

Figure 15. Hydrodynamic Gas Bearing Test Bed Parts

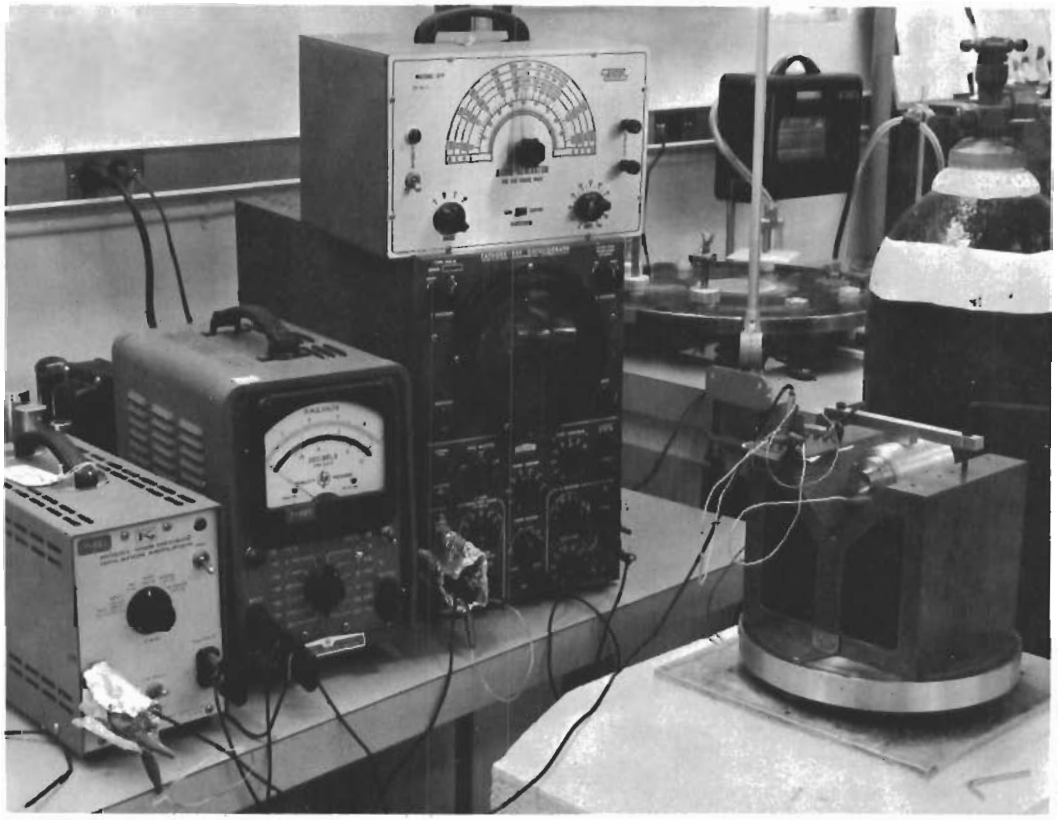

Figure 16. Hydrodynamic Gas Bearing Evaluation Test Setup

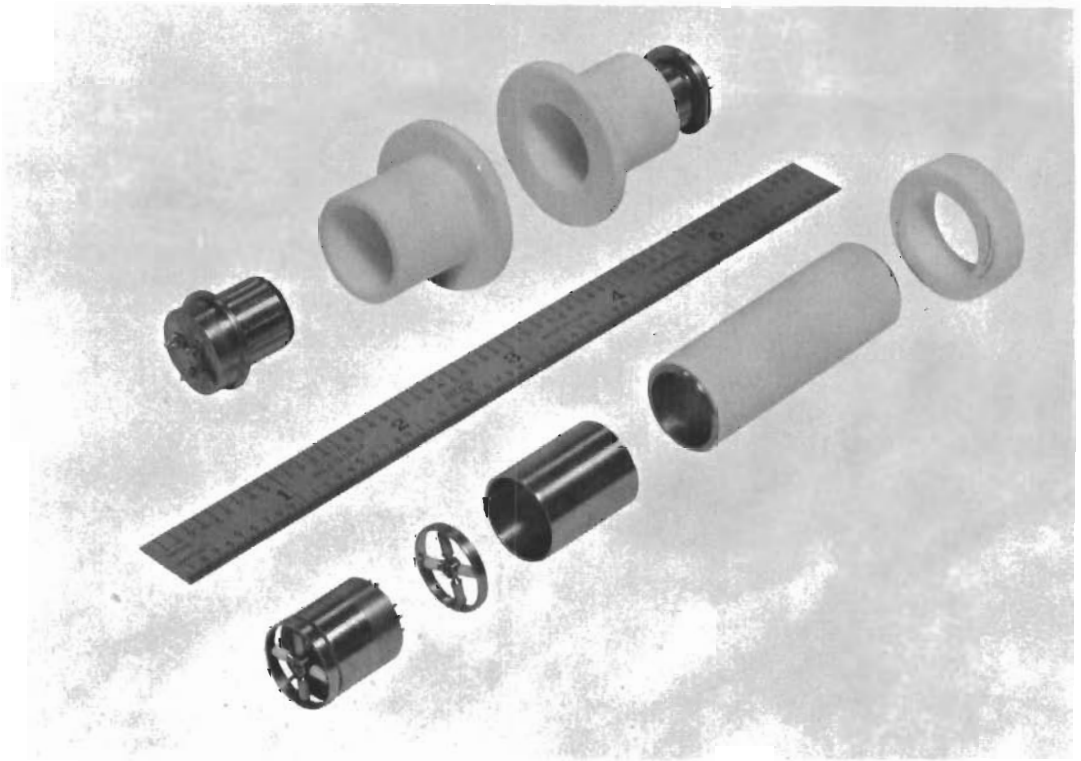

Figure 17. Prototype Hydrodynamic Gas Bearing Multifunction Sensor

The prototype gas bearing model was measured in terms of lift capacity in the two directions: power consumption for various gases, and the optimum motor gap configuration and power consumption.

Figure 18 indicates the performance of the bearing in a nitrogen gas environment for various spin velocities. The test setup was one utilizing a ball bearing coupled dead weight applied forcing function. The results of this indicated that there was 7.5 "G" capacity in the axial direction and 35 "G" in the radial direction. The bearing can easily be improved in the axial direction by a factor of three or four by additional work on the pumping plate proportions and size.

Figure 19 indicates the performance, in terms of power consumption, of the bearing when used with a low and relatively high viscosity gas. The spin axis drive in this test employed a prototype motor design with two stators using a nominal magnetic gap of .002 inches. The motor bearing combination used was capable of 12,000 RPM operation, and the later version with an improved geometry and motor was capable of 24,000 RPM.

The operation of the motor bearing combination with respect to power consumption is shown in Figure 20 for various motor magnetic gaps. The obvious purpose was to arrive at that gap which is most efficient for torque versus power consumption, with torque being the favored parameter. It is important that a reasonably large working magnetic gap be utilized to reduce the large radial pull in forces and the resultant starting problem. Fortunately, the hysteresis synchronous motor design used looked somewhat better at relatively larger magnetic gaps and the starting characteristics were easily satisfied. The magnetic gap eventually selected for the sensor prototype was .003 in., resulting in 50 gram-centimeters of torque at 15 volt-amps excitation.

2.5 NONCONTACTING CAPACITIVE SLIP RING

In order to compliment the possible long life of the gas bearing, an investigation into a non-contacting capacitive slip ring signal transmission system was made.

A test arrangement was first fabricated which involved a radial acting hydrodynamic gas bearing, simulating in size and proportion that which would occur in a final design, with a capacitive slip ring system integrated into it. (See Figure 21.)

The arrangement included a radial gap of 100 millionths and was part of a high impedance circuit driven from a crystal source instrumented to determine the noise and impedance of the joint under varying conditions. These conditions included effects due to:

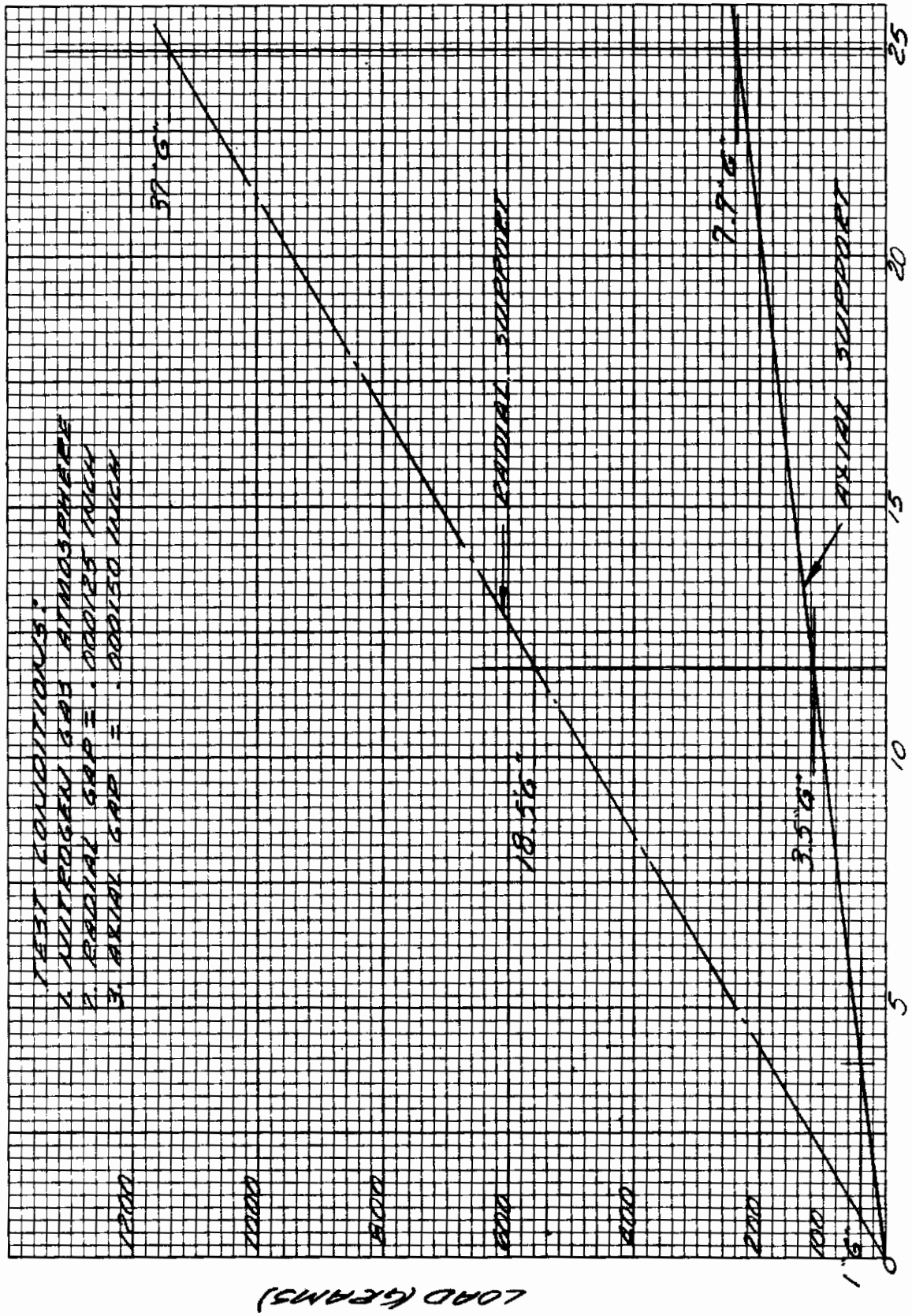

Figure 18. Gas Bearing Load Capacity at Various Spin Velocities

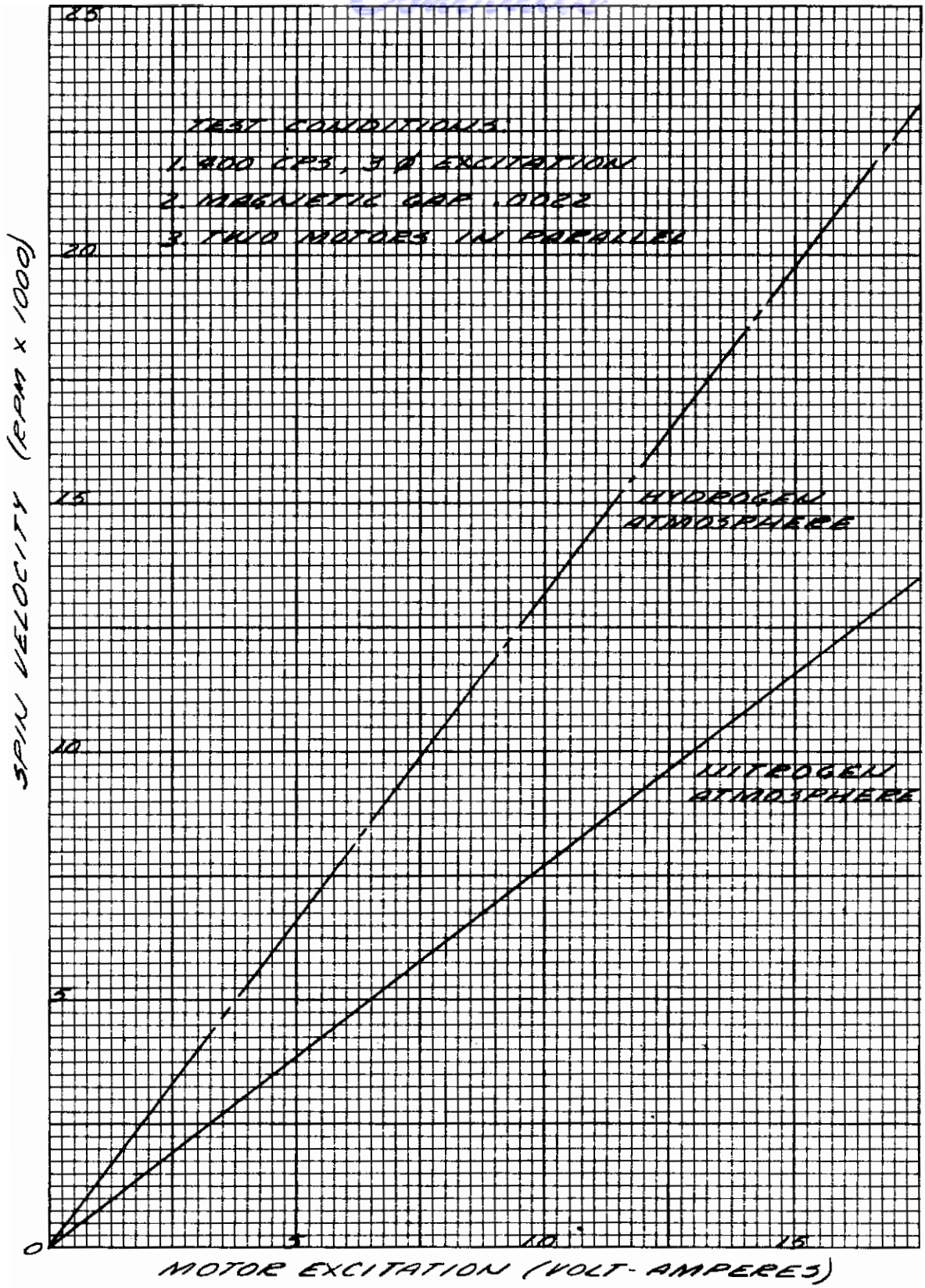

Figure 19. Spin Velocity vs. Power for Bearing Performance in Various Gas Atmospheres

Figure 20. Gas Bearing Spin Motor Performance

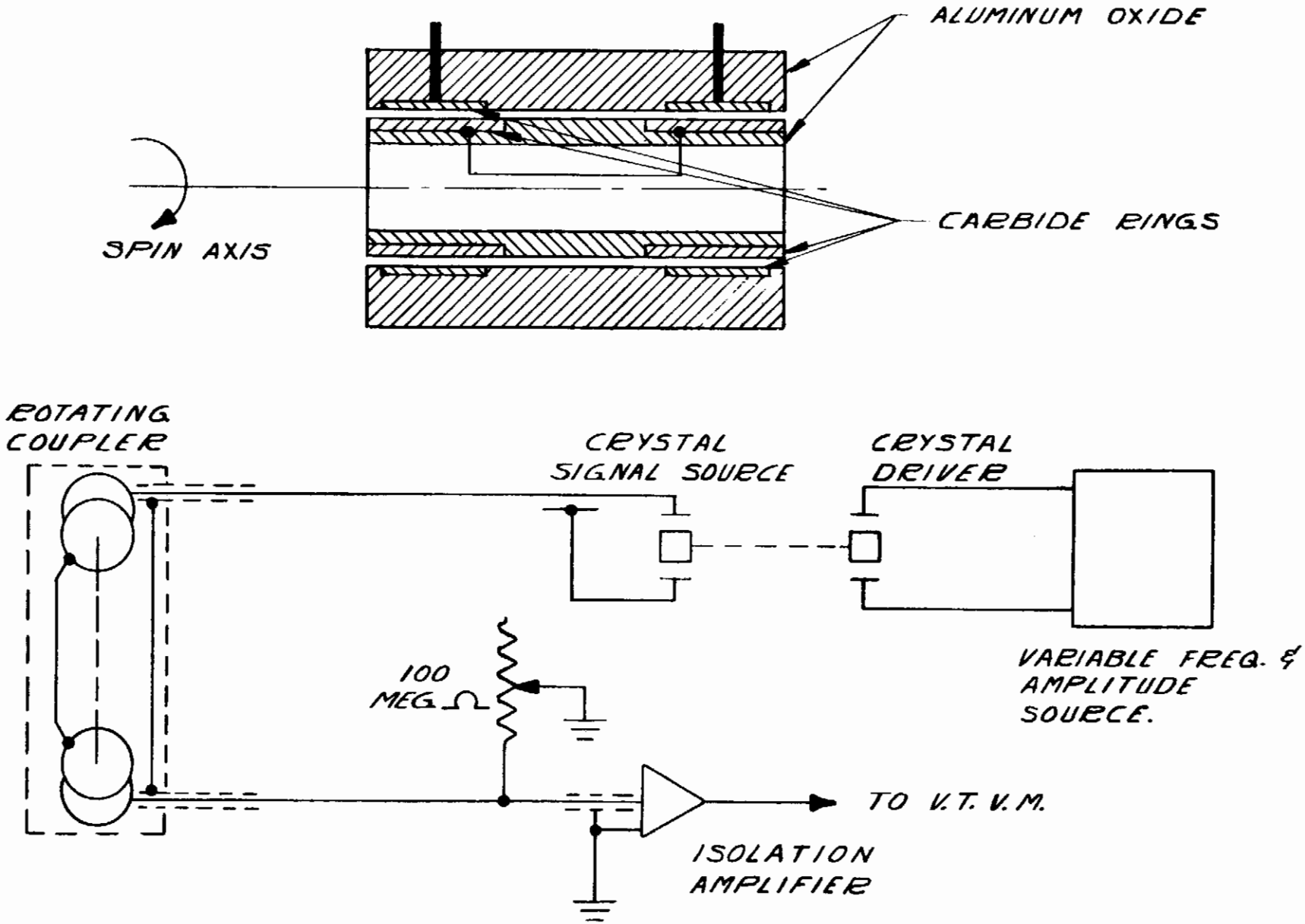

Figure 21. Non-contacting Capacitive Slip Ring Arrangement

a) Change in spin velocity.

b) Presence of magnetic fields.

c) Shielding effects.

The performance of the capacitive slip ring coupler can be summarized as follows. With the use of low permeability magnetic carbides in the capacitor ring there was no observable interaction with external magnetic fields measured at values of microvolts. Electrostatic generation caused by the remnant gas environment was in the order of 25 microvolts at 12,000 RPM, diminishing in an approximately linear fashion with speed. A 100 to 150 microvolt signal was observed at the fundamental frequency at 12,000 RPM, and appeared to be caused by external D.C. electric fields energizing the rotating capacitor in a generating fashion. The impedance of the joint at 200 cps was in the order of 5 megohms, which, in the sensing circuits to be employed, would not affect the gain seriously inasmuch as the isolation amplifier impedance is in the order of 50 megohms. The signal transmission device in this circuit, compared to the contacting arrangements previously used, represented a total noise reduction of 2 to 3 orders of magnitude.

A duplicate set of gas bearing parts with the added capacitor ring detail was fabricated and assembled utilizing the process previously described. The purpose of this assembly was to allow exact simulated measurements of the performance of the capacitor slip ring as a signal transmission device. This involved a dummy sensing cell, using a passive capacitor network, simulating the pickoff source installed into the gas bearing and hooked up in exactly the same way as if it were an actual cell.

For evaluation, a test arrangement, as shown in Figure 22, was employed which involved a sensor cell composed of two 250 pico-farad capacitors arranged in a circuit identical to that of a dipole pickoff, and encapsulated within a metal chamber. The outline dimensions and terminal board detail, lead paths, etc., were identical to that of the multifunction sensor cell. This single channel was connected to a pair of the slip rings with a metal shield insert simulating the motor rotor in place and the device set up in a gas drive fixture for running the spin axis.

The first tests involved the use of the dummy pickoff as a dead source load and measurements were made to determine the electrostatic generated noise within the capacitor slip ring. This test revealed a hitherto hidden characteristic of the arrangement - that of an electrostatic generator operating to build up a charge on the suspended member.

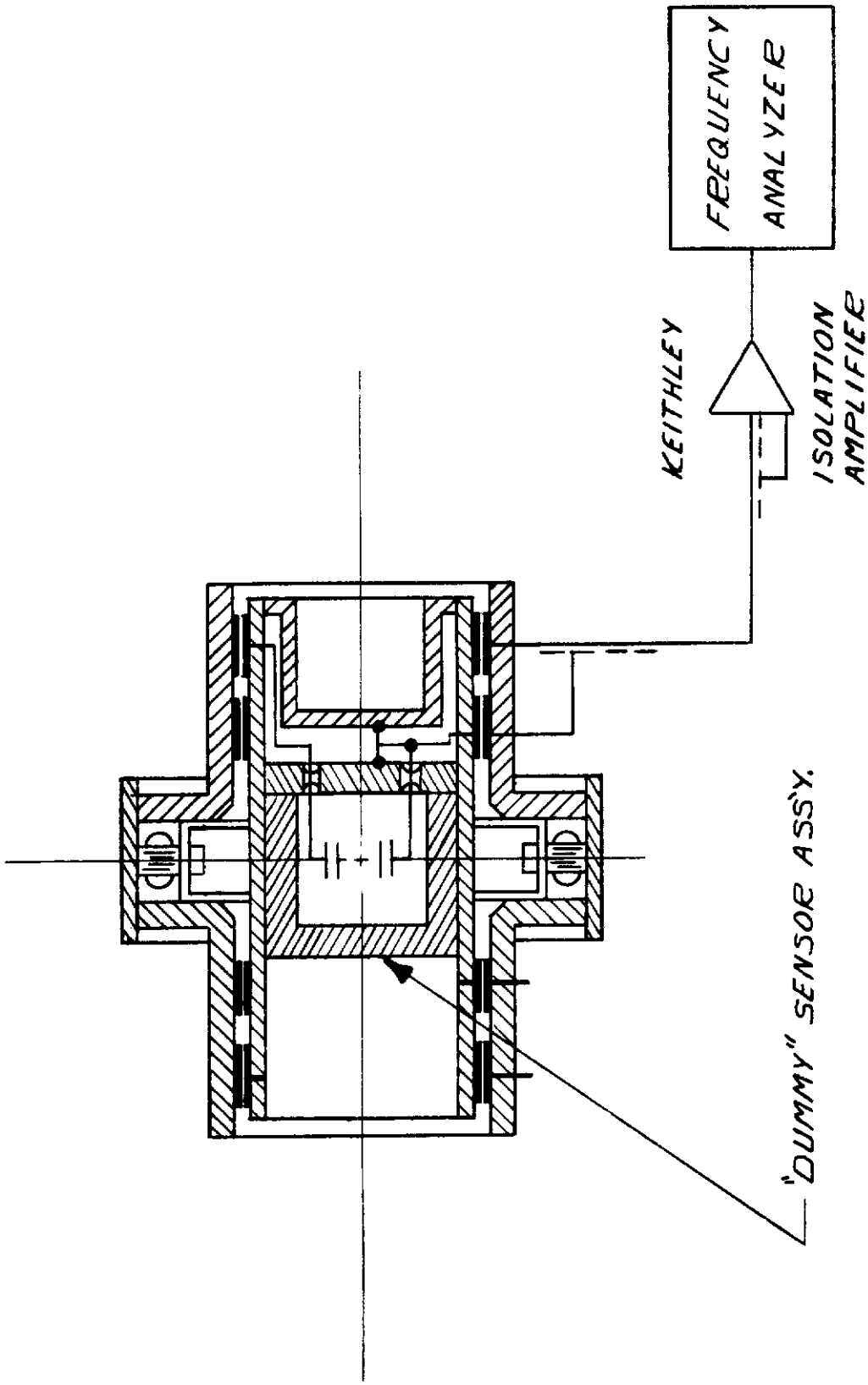

Figure 22. Capacitive Slip Ring Test and Evaluation Assembly

The effect operates as follows. With the system not spinning and the noise of the circuit noted, which obviously approaches zero within a few milliseconds after initiation of spin power and bearing lift-off, microvolt signal levels present in the circuit started to build immediately to some value determined by three physical constants: spin velocity, dielectric gas gap and the dielectric constant, and work function characteristics of the gas in the gap. The effect of this electrostatic generation operated to generate an A.C. voltage which was identical to the spin frequency, phase locked to the spin body, and with a magnitude which was the integral of the spin velocity over time. In other words, the total distance travelled by the spin body was proportional to the A.C. analog present at any moment. This mechanism saturated in the conditions described above, with the dead body crystal at a level of 150 millivolts RMS for a terminal spin velocity of 12,000 RPM, and at a level of 300 millivolts for 24,000 RPM. It is postulated that the electrostatic charging effect was caused by an ionic unbalance due to the "scuffing" of the gas molecules within the bearing film. Because there was no conductive path across the joint, there was a net D.C. field built up between the metal parts comprised of the sensing cell and the capacitor plate on the rotor, with the ceramic substrate acting as a dielectric member. Inasmuch as the source was a capacitive coupled device, there was no terminal equalization so that the charge could thus build to some value determined by the electric breakdown of the gas film.

Because the capacitor slip ring was a continuous cylinder (not segmented), the buildup of an A.C. voltage, which was phase locked to the spin body, indicated that there was an equivalent of an electrostatic dipole affixed to the spin body with a unique and fixed angular orientation. This came about because of the assymmetries in the electrostatic pattern affixed to the rotating member, inasmuch as in this model the moving electrode would not overlap the fixed electrode in the longitudinal direction.

Although this electrostatic charging of the rotary member was of potential usefulness as an integrating technique, it also proved to be a serious limitation on the usefulness of the capacitive slip ring arrangement. Additional techniques may well enable this non-contacting slip ring arrangement to work; but, the length and intensity of such an investigation had to be foregone in favor of more immediately pertinent work in this program.

3. TEST AND EVALUATION EQUIPMENT

To evaluate the prototype multifunction sensor, a test complex was assembled, modified and supplemented throughout the program. A brief description of the test and evaluation plan and associated equipment is as follows.

The overall test and evaluation plan, described in Figure 23, dictated the generation of several unique test setups. Included was a complete test and evaluation console to operate the unit and monitor all of the major parameters continuously. (See Figure 11.) In addition, a recorder suitable for displaying the resolved and demodulated inertially derived information was included.

To furnish a precise physical reference system, a granite measurement block was installed on the measurement pedestal with means for leveling. (See Figure 12.) This setup allowed rotation around a vertical axis without changing the "G" coupling significantly, thus permitting the use of the local horizontal earth rate component to be used as the rate input for threshold measurements on the rate sensor.

A 15° per increment plunging head was used to tumble the sensor about a horizontal axis. The precision of this device permitted linearity measurements on the accelerometer to within ±.001 "G", which was well beyond the linearity limitations of the readout instrumentation.

Figure 24 depicts the elements and arrangement involved in the readout instrumentation setup. The isolation amplifier following the transducer was mounted immediately adjacent to the output on the plunging head, the whole of which was covered with an electrostatic shield. The total vector, unfiltered signal at unity gain was lead through an umbilical cable to the test console where filtering and gain was added, the output of which operated the demodulators in the phase angle voltmeter for direct readout and recording.

During the course of this phase of equipment buildup, an angular oscillation table was also designed and fabricated suitable for making dynamic angular response measurements. This table permitted inputs from .01 cps up to 20 cps at peak angular velocities of 10°/hr. to 10°/sec., and included a suitable angle transducer integrally mounted for motion readout. (See Figure 25.)

During the latter part of the program certain revisions, refinements and additions to the test complex were made. They included:

a) The completion of the overall operational control panel including a complete readout system for monitoring temperature, reference generator outputs, motor inputs, and D.C. power. Also included was a power supply stabilizing element.

b) A four-channel recording system, including demodulators and D.C. plug-in preamps suitable for the simultaneous recording of all major effects and outputs, was provided. A wide band North Atlantic Phase Sensitive Voltmeter capable of operating at carrier frequencies of 20 cps to 100 KC was utilized.

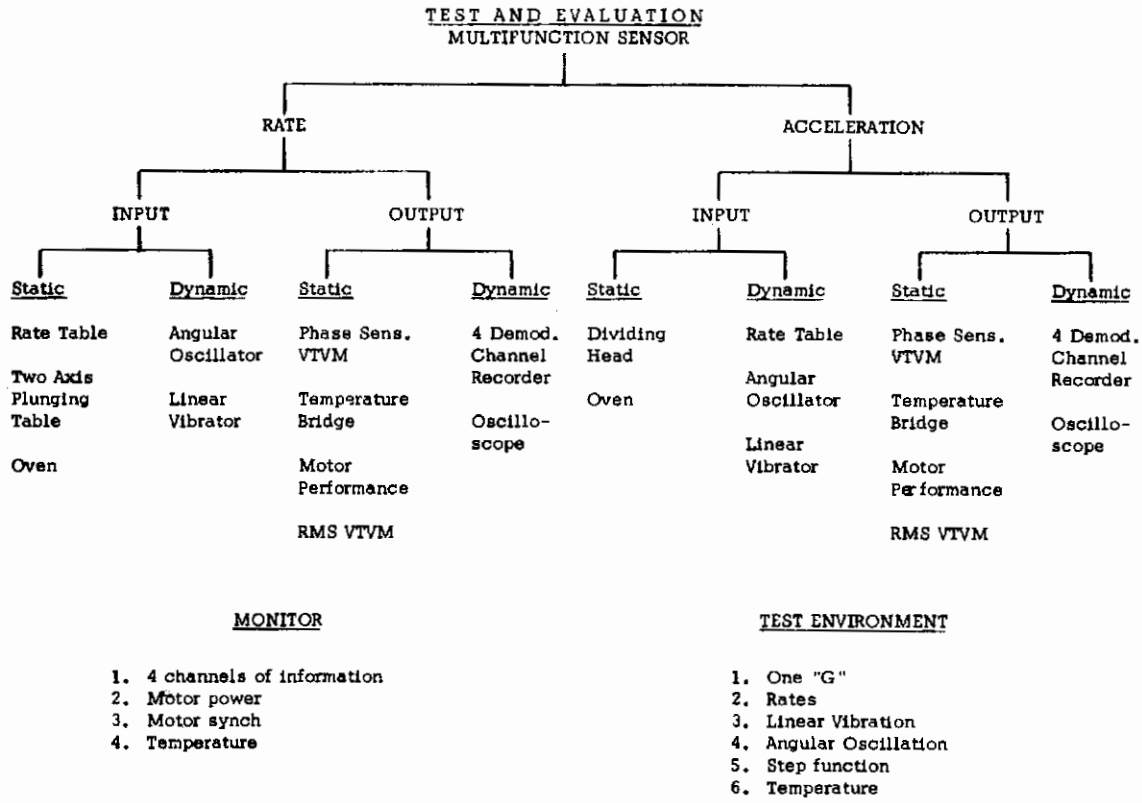

Figure 23. Test and Evaluation Plan

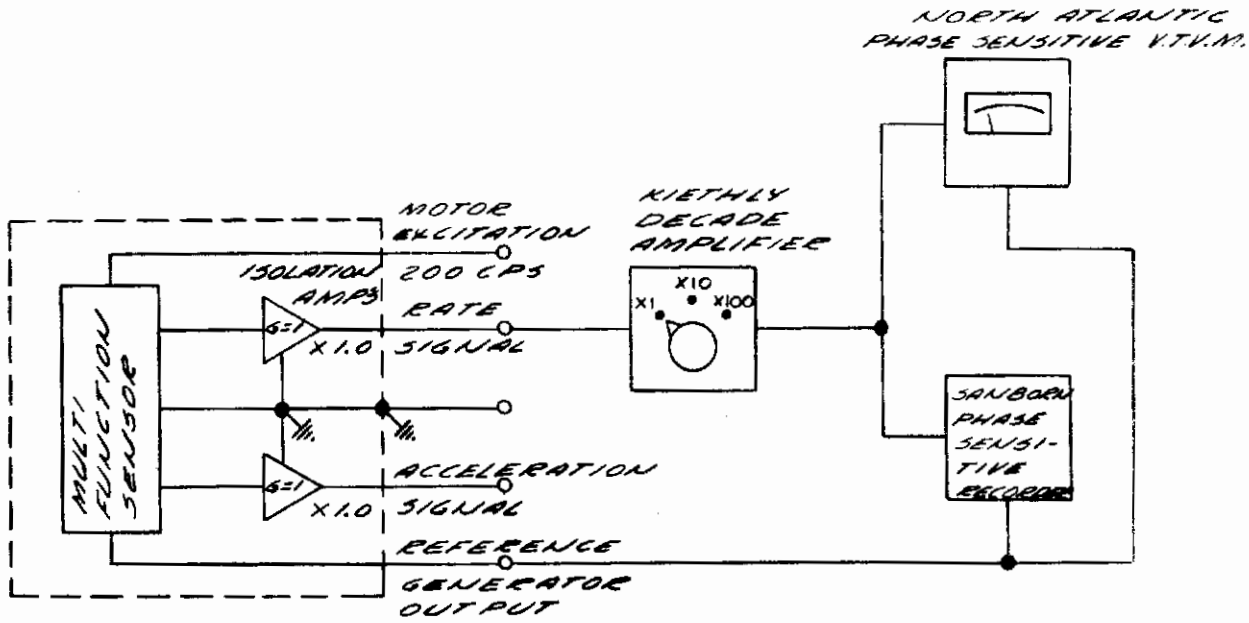

Figure 24. Readout Instrumentation Setup

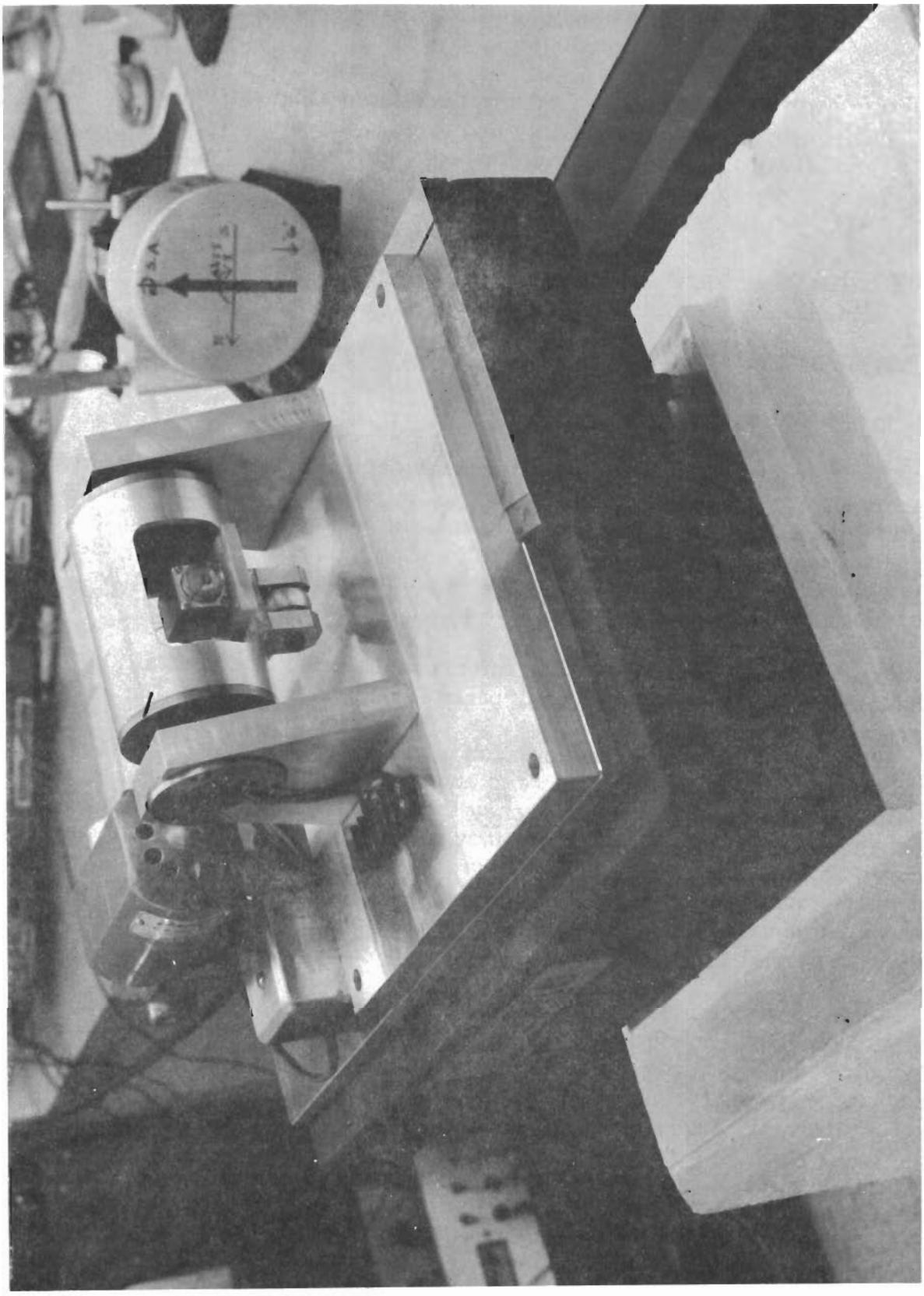

Figure 25. Angular Oscillation Table

In addition, a Keithley Decade Isolation Amplifier with selectable band pass filtering inserts allowed operation from 200 to 1,000 cps.

c) In an effort to further reduce the mechanical background noise uncertainty and to allow more measurement flexibility, a new concrete pedestal steady-rest was poured and a granite capstone for leveling and reference surface was installed.

4. FINAL ASSEMBLY AND EVALUATION OF GAS BEARING MULTIFUNCTION SENSOR

4.1 ASSEMBLY

4.1.1 Multifunction Sensor Cell

The first model prototype multifunction sensing cell was demonstrated in a ball bearing suspension system. This initial evaluation involved the fabrication and assembly of two new multifunction sensing cells with a test series performed on one sample in the ball bearing suspension system, the purpose of which was to correlate data between the operation of a relatively low frequency rate sensing pickoff versus a high frequency unit.

Figures 26 and 27 describe the effect on scale factor and total RMS null when the pickoff natural frequency parameter is varied by 3 to 1.

Referring to Figure 26, the multifunction sensor rate element resonates at approximately 700 cps in the fluid and under dynamic conditions. This compares with a 1,600 cps resonant frequency for the standard sensor. The scale factor change due to the resonant frequency rise begins to exhibit the characteristic curve between 300 to 700 cps. Since it was difficult to predict the coupling "Q" of the mercury to the sensing crystal assembly by extrapolating from one sensing cell to another, it was necessary to perform such a test series to determine the effect on natural frequency of the mass and crystal spring rate combination.

Referring to Figure 27, the same two sensors evaluated in terms of the total RMS A.C. null show a sharp drop at the resonant point for the low frequency unit, which is in the predicted direction. In other words, operation in the resonant mode acts to increase the scale factor at the same time decreasing or filtering the null, excluding frequencies other than fundamental.

The purpose of this series was to inspect the performance potential of this arrangement for extreme low threshold detection with limited dynamic range where the device would be utilized in stabilization applications.

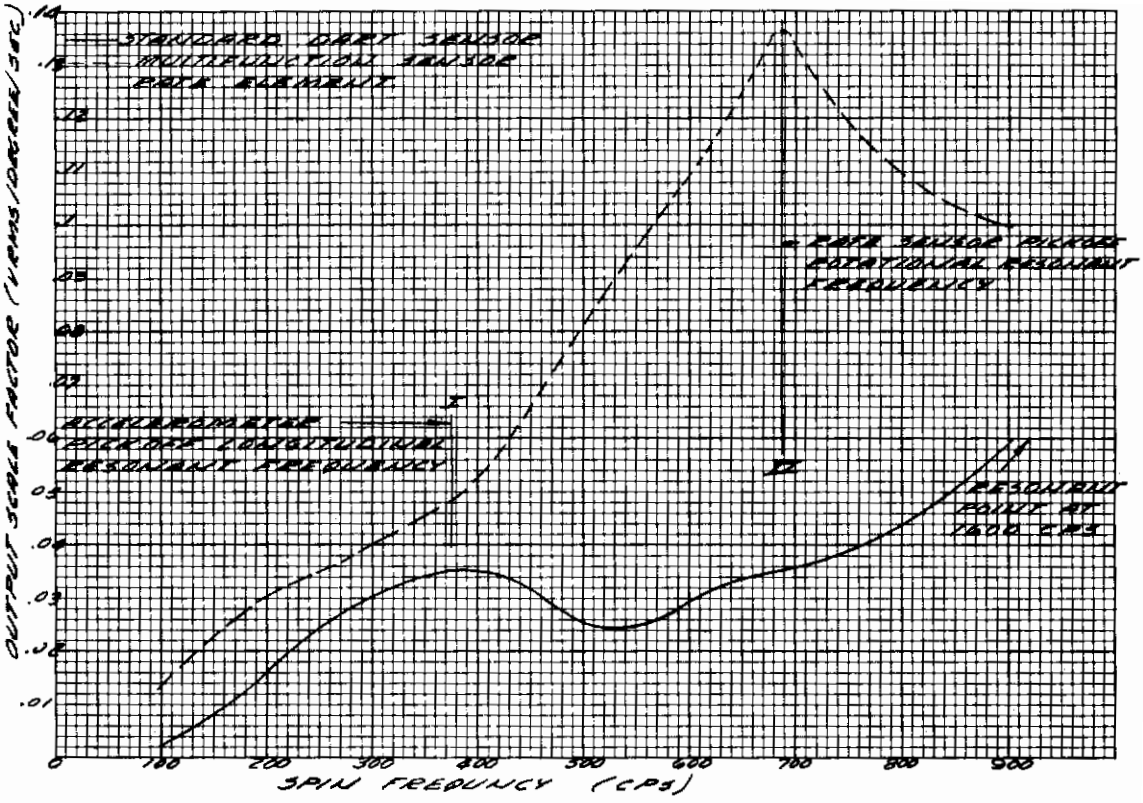

Figure 26. Rate Sensor Scale Factor vs. Spin Velocity

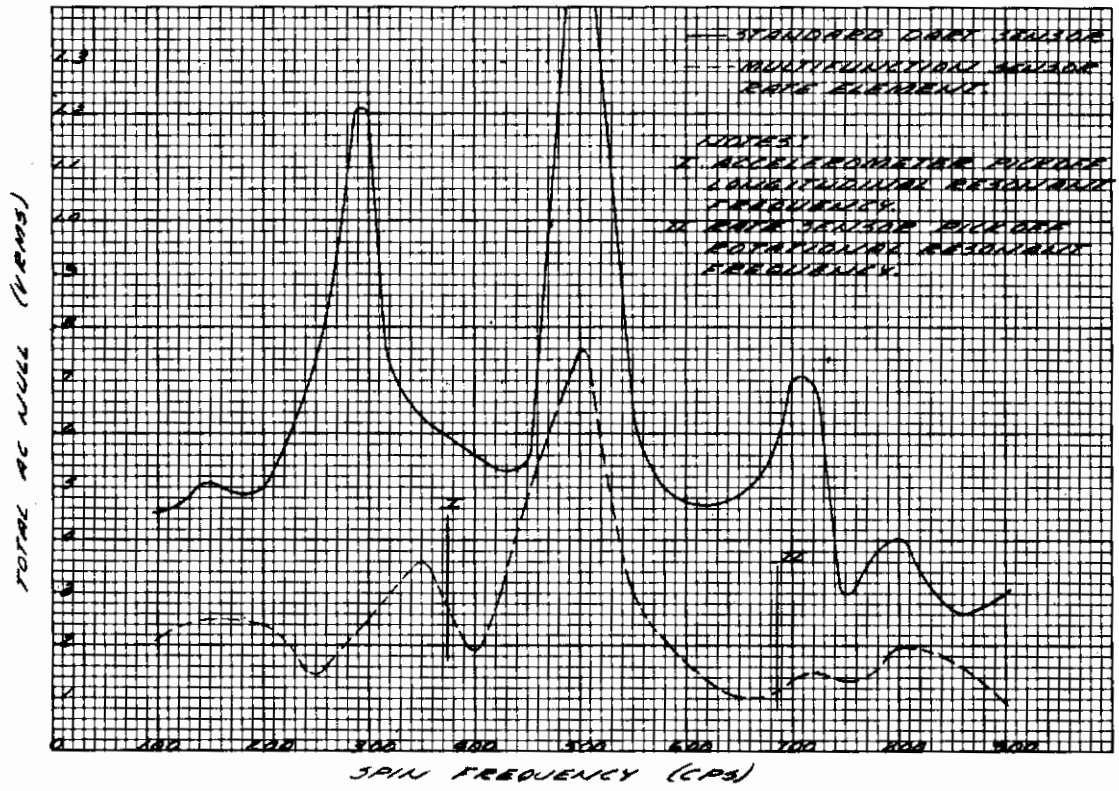

Figure 27. Rate Sensor Null vs. Spin Velocity

A second prototype high frequency multifunction sensing cell was fabricated and assembled into the first gas bearing prototype.

4.1.2 Multifunction Sensor

Subsequent to the assembly of the multifunction sensor cell into the hydrodynamic gas bearing rotor pumping plate assembly, it was necessary to design, fabricate, assemble and operate a hydrodynamic gas bearing fixture suitable for use in the spin axis balancing machine. With the successful conclusion of this series, the spin axis assembly was balanced with attention given to balance in the operating range of 12,000 to 24,000 RPM. The unit exhibited a balance control which operated at near the ultimate capabilities of the balancing machine, which was in the order of .003 drill depth material removal, on a 40 thousandths diameter drill, with a spin speed of 200 cps.

Subsequent to this operation, the balanced spin axis assembly was introduced into the gas bearing outer frame using previously prepared tools, including a V block fixture which held one motor stator into position to drive the spin axis during the bonding cycle. This method for assembly proved itself on several occasions to be reliable, extremely repetitive and very economical to use, inasmuch as no precision tools were required.

The final assembly resulted in a radial gapping in the order of 200 millionths. Also installed at this assembly operation was a single phase stator to act as a reference signal generator. A major consideration for the assembly technique was that with one motor stator in position at the final assembly stage, a summary of the torque requirements was obtained with complete monitoring of the operation of the spin bearing during the bonding cycle, thereby eliminating any misalignment errors. In other words, the spin bearing motor combination must operate normally before, during, and after the final assembly cycle without significant change. Figure 28 shows the layout before assembly of end covers and case.

After the final assembly of the bearing combination and testing to determine power requirements, etc., the motor stators were introduced using the same fixture, and, while operating in a dynamic condition, bonded into place, thereby resulting in the semifinished multifunction sensor bearing combination. At this point the assembly was essentially closed to dirt contamination and reasonably easy to handle. (See Figure 29.)

Because of the unknown thermal aspects of the unit, a test series was run to determine approximately the effects of clamping on the unit to establish the best method for mounting in any given installation. It was soon determined that, in general, it was best to clamp the unit at the C.G. point because, under these conditions, there was the least amount of thermal gradient introduced across the bearing interfaces. During the course of these tests, which employed

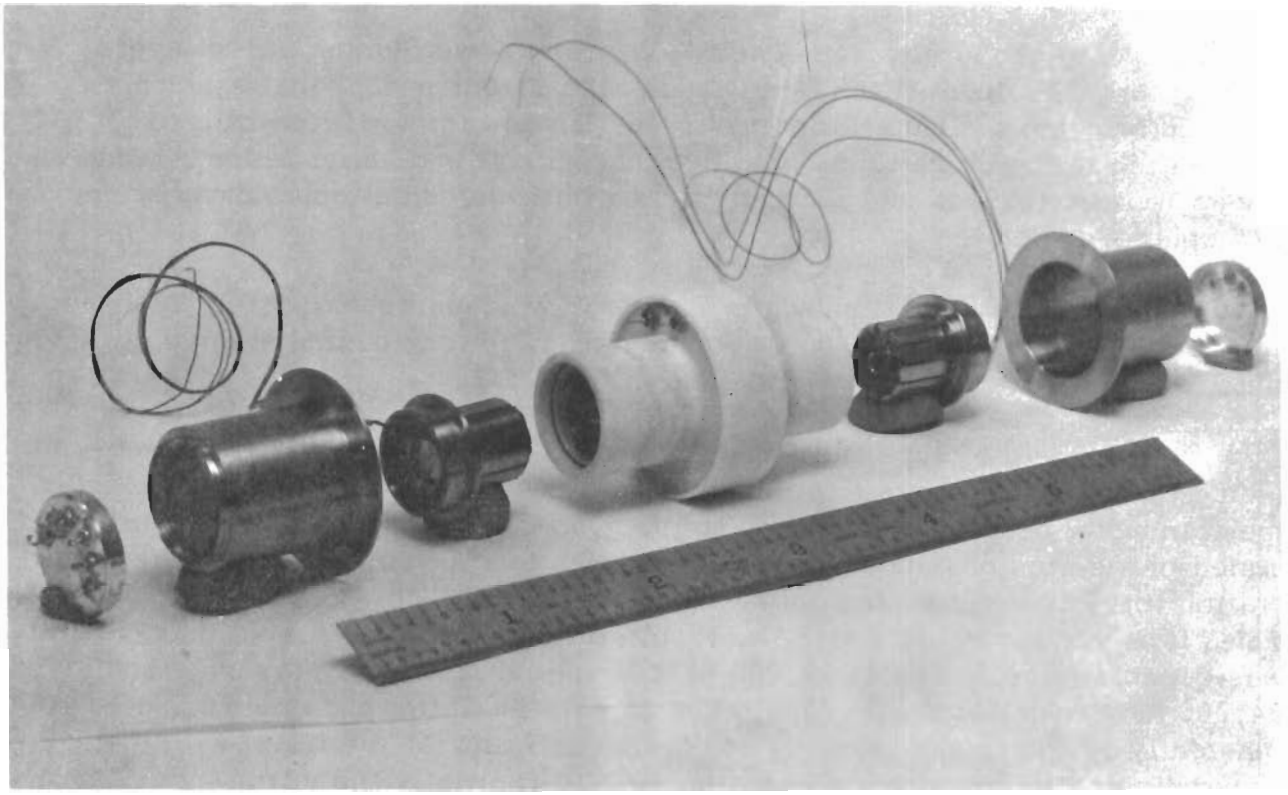

Figure 28. Multifunction Sensor Exploded View Assembly

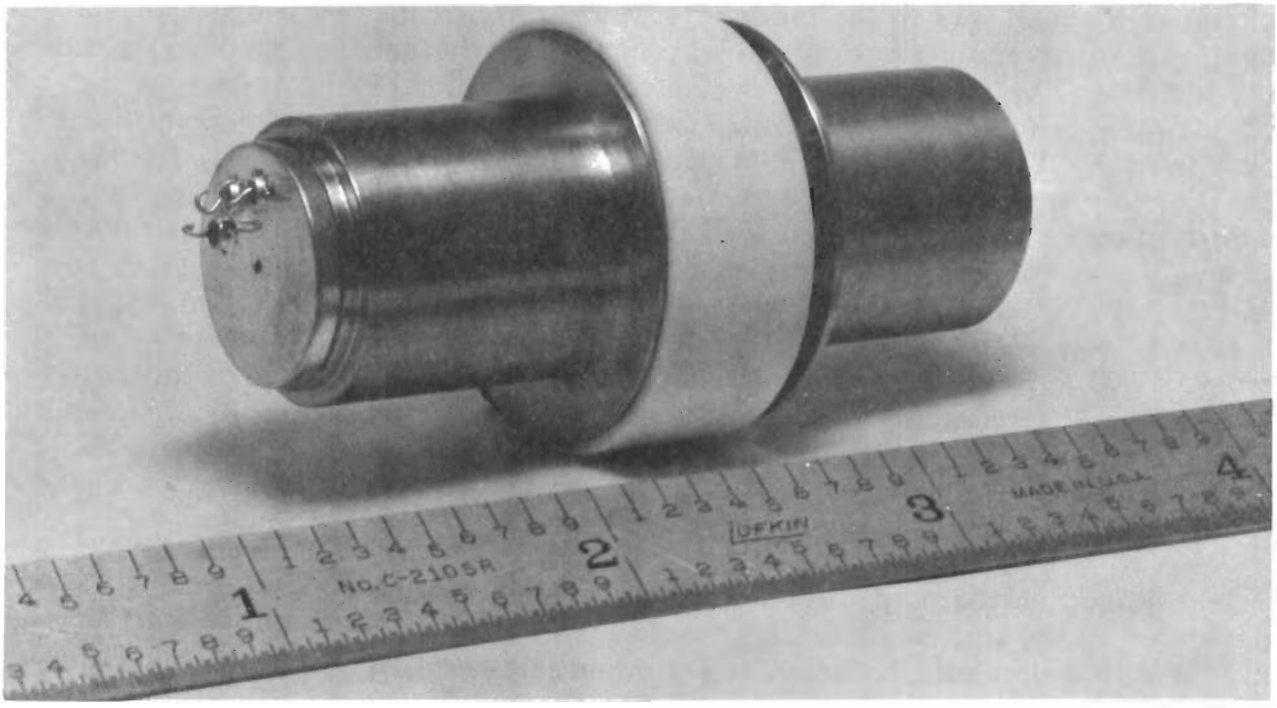

Figure 29. Multifunction Sensor - End Covers Installed

helium, hydrogen and nitrogen gases - operating power versus speed levels, starting torques, coast times, etc., were also determined. Final assembly included bringing the metallic hermetic seal covers into position with the installation of the brush block on the signal pickoff end, after which the end covers were introduced and the unit filled with hydrogen at approximately one atmosphere.

The completed unit shown in Figure 30 weighed approximately 115 grams with a major diameter of 1.3 in. x .55 in. in length, and a minor diameter of .8 in. x 2.5 in. in overall length.

After the prototype multifunction sensor was assembled, it was subjected to a series of tests to determine the final operating characteristics of the spin motor bearing combination in the hydrogen atmosphere. This consisted of a series of runs at various excitation levels while determining acceleration time, power consumption, voltages, currents, etc., as well as coast times from various velocities. The results of this series indicated that the unit was capable of operating at 12,000 RPM with adequate torque reserve, and at 24,000 RPM with marginal torque reserve, with the latter case being limited not inherently by the torque reserve, but by the thermal rise attendant with the power dissipation required to operate. Because initially the exact spin velocity was not important, except for considerations having to do with frequency response characteristics, it was felt that the selection for the best running speed would result from an analysis of the drift characteristics or error producing elements in the sensor proper. Subsequently it was determined that the upper end of the spin speed was in the order of 16,000 RPM and the lower end at 8,000 RPM, the lower end being determined primarily by the sensing mechanism and the higher end being determined by the tolerable thermal rise. Operation at 12,000 RPM resulted in the following characteristics for this spin motor bearing combination. For starting, 7.6 VA power was required which operated to bring the unit to speed in 2.7 seconds. Under these excitation levels, after having achieved sync, the power input requirements could be reduced to as little as 1.8 VA before dropout. The unit remained in sync at a power consumption of 4.9 VA but 7.6 VA was required to overcome the starting friction. This means that in some modes for starting - high power impulses could be put in (in the order of 200 milliseconds) with subsequent cutback to the normal operating power levels. At a terminal velocity of 12,000 RPM the unit required approximately 18 VA to achieve sync and ran nominally at 15 VA, with dropout occurring at approximately 5 VA; however, at these excitation levels the thermal rise began to be excessive, unless properly heat sinked.

Based on the preceding motor bearing thermal measurements, it was decided that the initial evaluation would involve the speed range of 8 to 16,000 RPM with the first runs to determine if other parameters would tend to select a specific operating frequency.

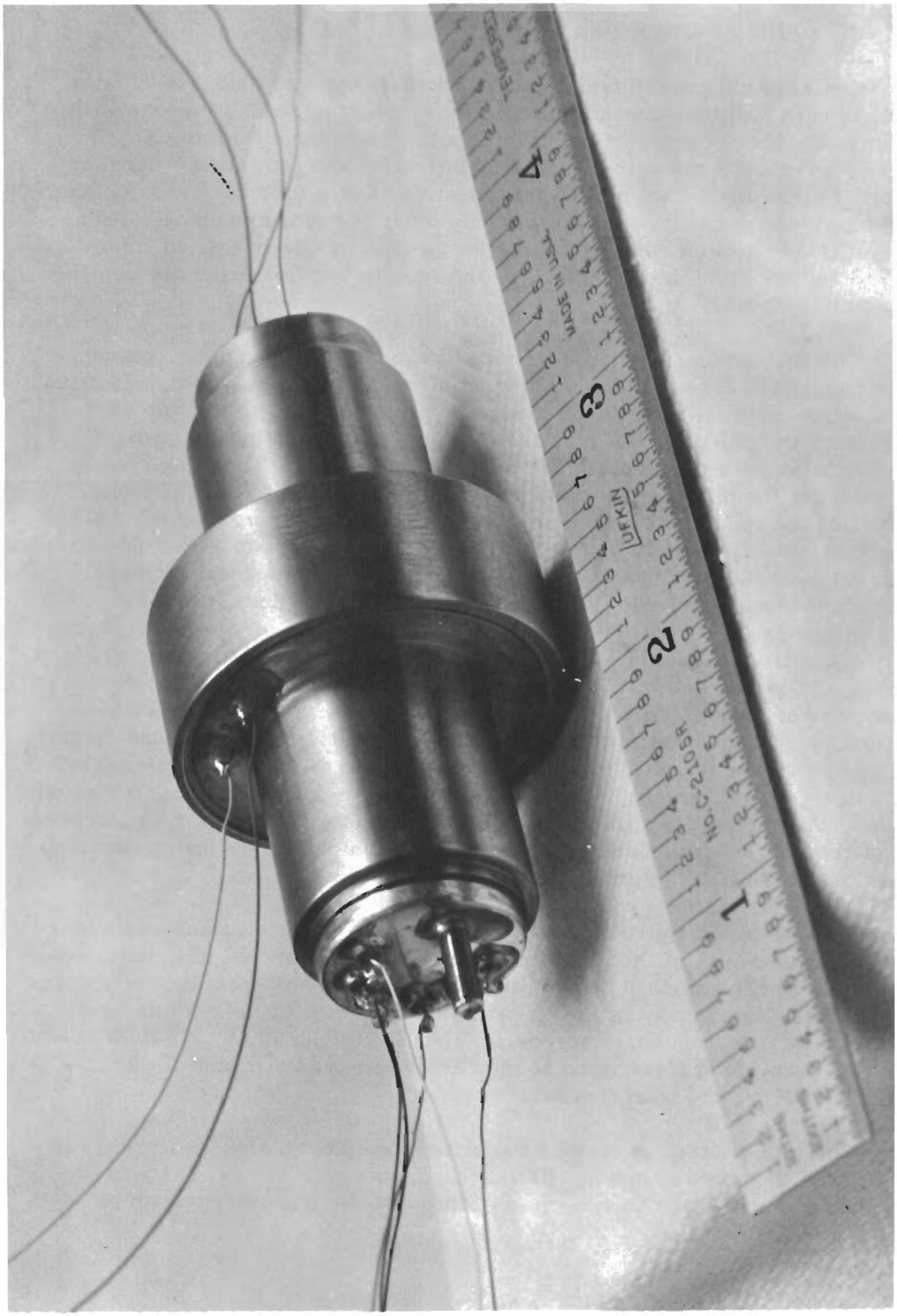

Figure 30. Multifunction Sensor - Final Assembly

4.2 TEST AND EVALUATION

The assembled prototype multifunction sensor was next set up on a rate table with a plunging head suitable for establishing the spin axis with respect to the local vertical field in the various positions (Figure 31). A series of tests were run on both the accelerometer and rate sensor portions to determine the total RMS null characteristics, scale factors, cross coupling inputs, electrical cross talk, and any other peculiar dynamics This series of tests was run with the spin speed as a variable operating from 8,000 to 16,000 RPM, incrementally. The results of this series are depicted in Figures 32 and 33.

The test setup included a variable frequency, three phase, power supply to operate the spin axis in snychronism at the various spin velocities, two isolation amplifiers to match the instrumentation load to the sensor's output, and an AC RMS VTVM and oscilloscope for monitoring the pickoff outputs. With respect to the null, the information in Figure 31 is depicted as a band showing the high frequency excursions from second to second which occurred at the readout point. The value of the null at approximately 12,000 RPM and its stability indicated approximately three orders of magnitude improvement over that of the operation in a ball bearing suspension system. The scale factor was normal with no unpredicted characteristics. The plot in Figure 32 indicating the total null plus one "G" input, with an attendant discontinuity occurring at roughly 12,000 RPM and thereafter linearily decreasing at higher speeds, was due to the following. The present standard rate sensing element has an expansion void, or bubble, in the mercury fluid cell which experiences an "equalization" process from the stress induced by the centrifugal field and, in general, is a step function, due to the large internal molecular forces of the mercury, i.e., surface tension. Subsequent to its "equalization", the unit will exhibit more or less pendulocity, due to the misplacement of the ball bearing member, the effects of which reduce with increasing speeds in terms of "G" sensitivity.

The prototype multifunction sensor accelerometer element was evaluated similarly to that of the rate sensor, in terms of the total RMS null, scale factor, and inertial cross talk from angular inputs. These results are shown in Figure 33. Noteworthy is the changing scale factor of the accelerometer with the operating frequency increasing linearly from 8,000 to 9,500 RPM and thereafter decreasing linearly to 16,000 RPM. The scale factor of 600 mv/"G" at 24,000 RPM agreed with previous tests.

The null characteristics of the accelerometer, in any speed range observed, was improved enormously over that of the ball bearing suspended arrangement - amounting to two orders of magnitude of transferred noise reduction.

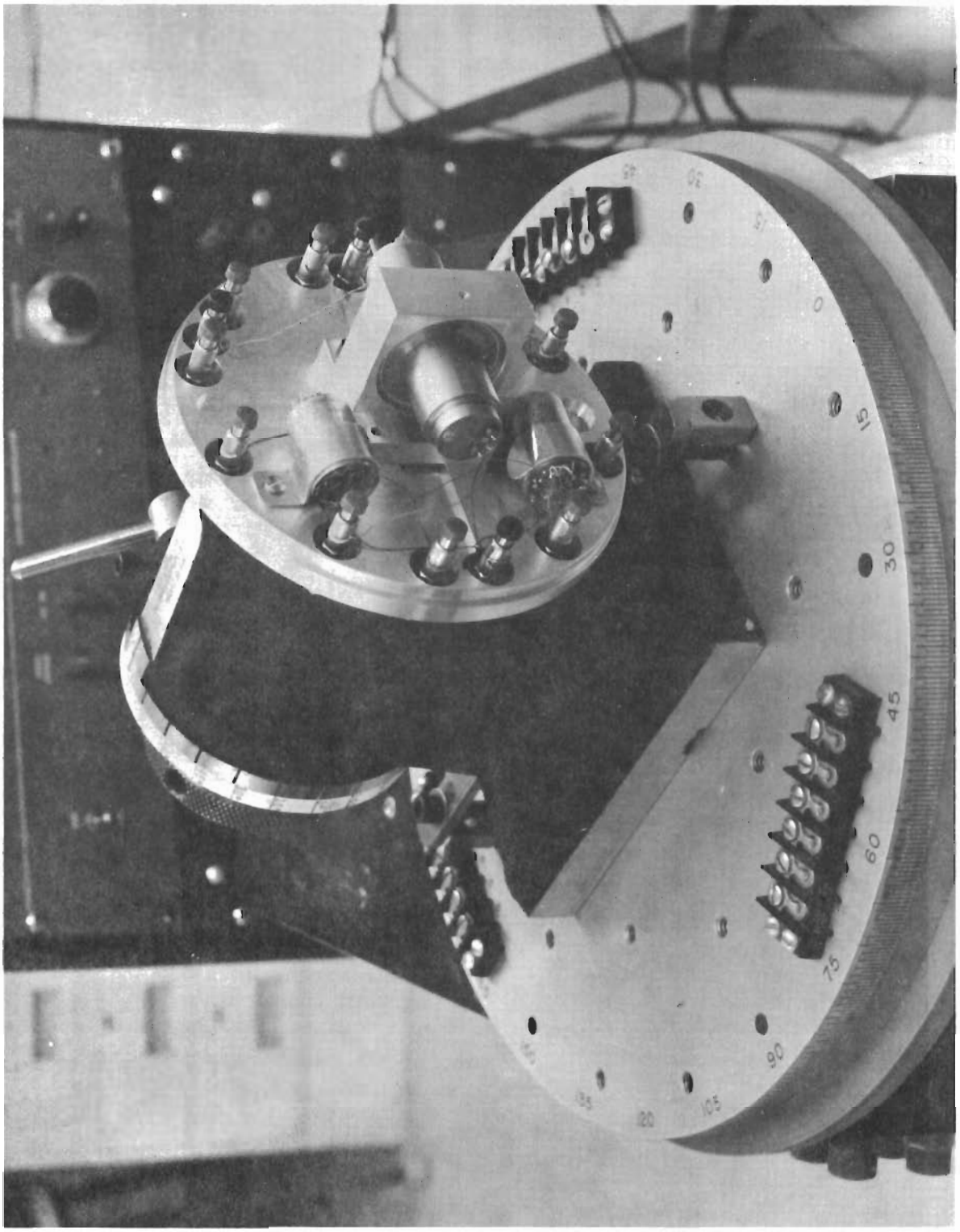

Figure 31. Plunging Head Setup on Rate Table

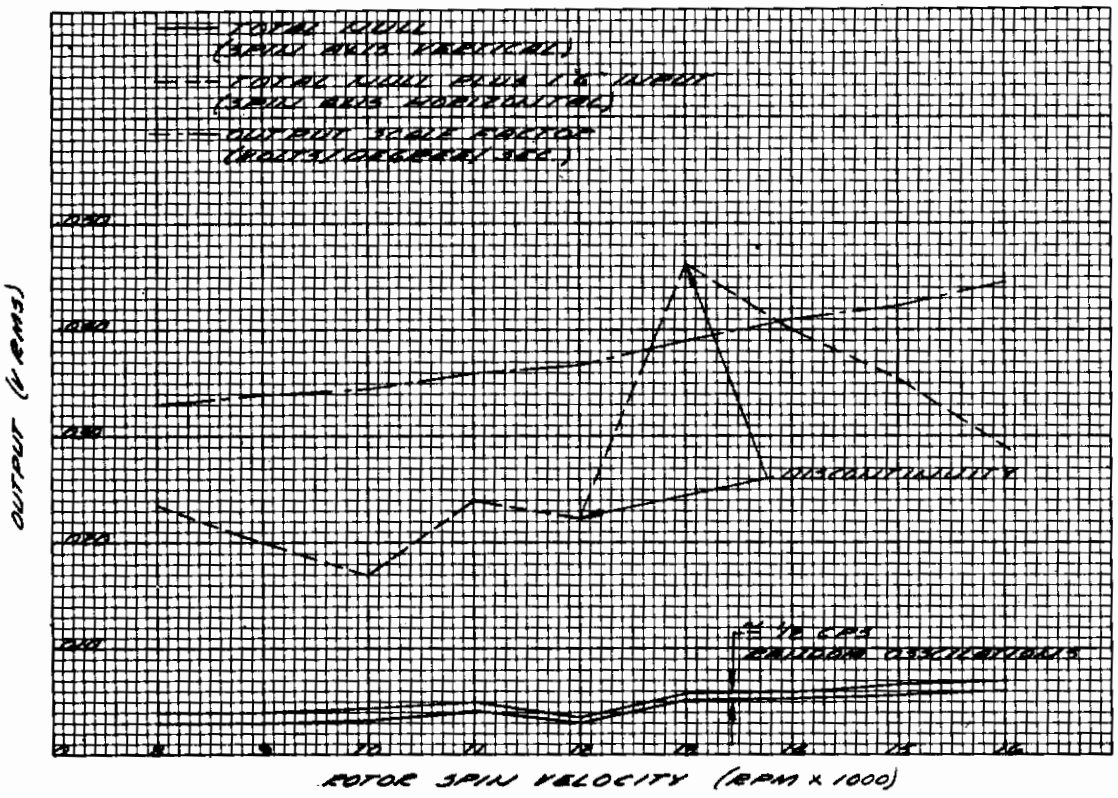

Figure 32. Multifunction Sensor Null Output Performance

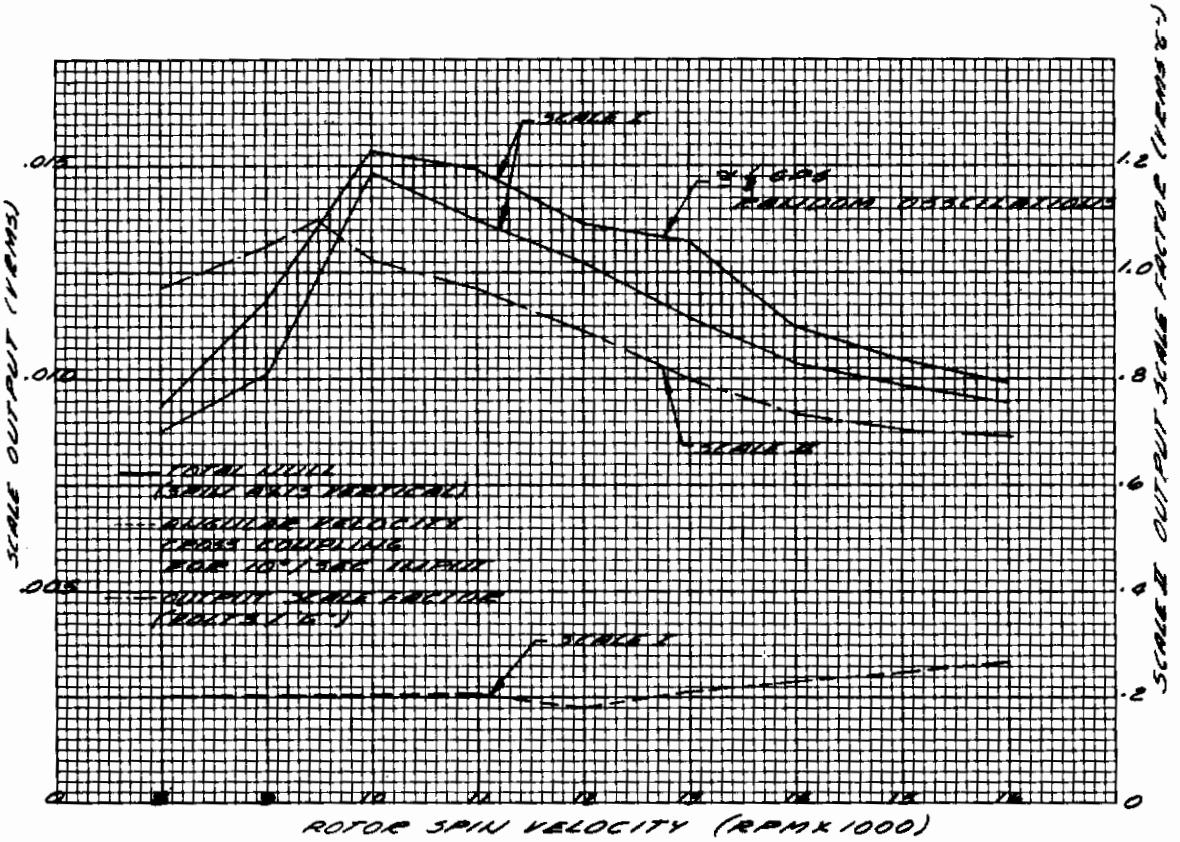

Figure 33. Multifunction Sensor Scale Factor Performance

The accelerometer output from an applied angular velocity input indicated a coefficient of approximately .0001 "G"/deg/sec. which was very good considering that no final tuning or trimming was required.

A step-by-step elimination of the electrical and electronics induced uncertainties occurring in both the immediate area of the transducer mount as well as in the control and readout equipment was made. These tests involved the transducer running normally instead of the crystal pickoff outputs driving the two readout channels, shielded dummy capacitors simulating the crystal's impedance source, and in every way shielded to simulate it, were substituted directly at the input probe to the isolation device. Every attention possible was given to provide exact simulation of the electrostatic environment. The results of this are depicted in Figures 34 and 35.

A series of recordings were made on the two outputs, one hour with the inertial sensor output device recording its null uncertainty, followed by one hour with the simulated crystal source inserted in place of the crystal pickoff. An inspection of Figure 34 showing the rate sensor element performance with a full scale readout equivalent to 5°/hr. indicates that total null uncertainty could be included in an envelope equivalent to 1.75°/hr. An inspection of the lower four elements in this same figure shows that the same recording channel with the dummy crystal inserted had a total noise band width of 1.1°/hr. with a frequency distribution similar to the active rate sensor. This indicated that even with the recorder loop gain at 4,000, the transducer threshold was still well into the null uncertainty of the test equipment.

The corresponding set of results, depicted in Figure 35, for the accelerometer channel, while showing the same characteristics, are proportionately not so limiting because of the higher scale factor of the accelerometer. In this case the recorder loop gain was 400 rather than 4,000 as in the case of the rate sensor. Operating at these sensitivities, the null uncertainty of the accelerometer began to be quite recognizable over the null uncertainty of the readout equipment with its average value something less than .0002 "G's".

At that point it was not recognized whether the accelerometer's performance was limited by the transducer or the remnant mechanical environment.

Since these tests of the thresholds of the two transducers revealed them to be below 1°/hr. and 10^{-4} "G's", no further attention was given to establishing more exact threshold limitations inasmuch as other instrument parameters were then more important. Notable among the parameters then to be tested were the "G" sensitive term, linearity measurements and the larger long term null uncertainty character of both outputs under temperature.

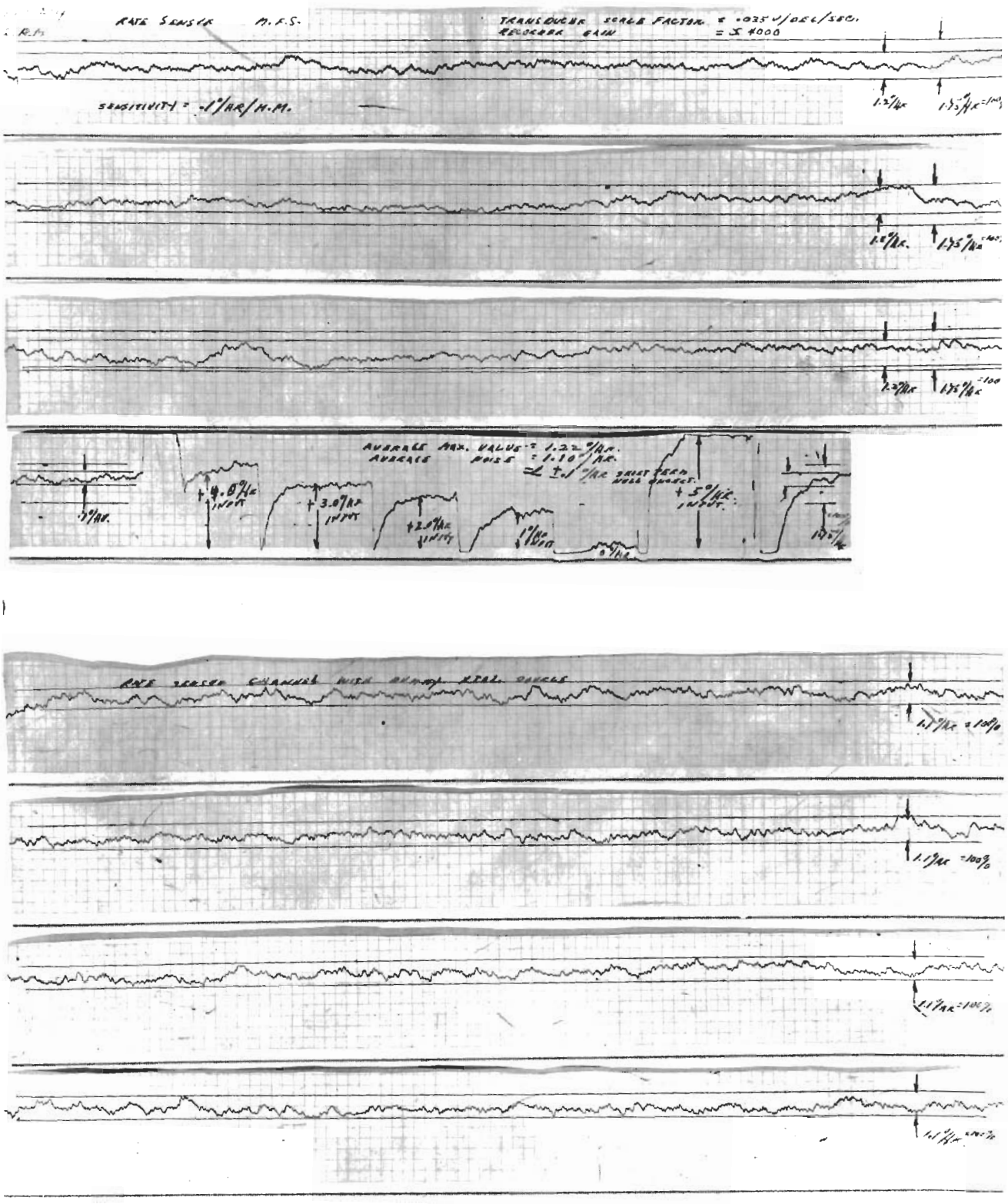

Figure 34. Recorded Test Data - Accelerometer

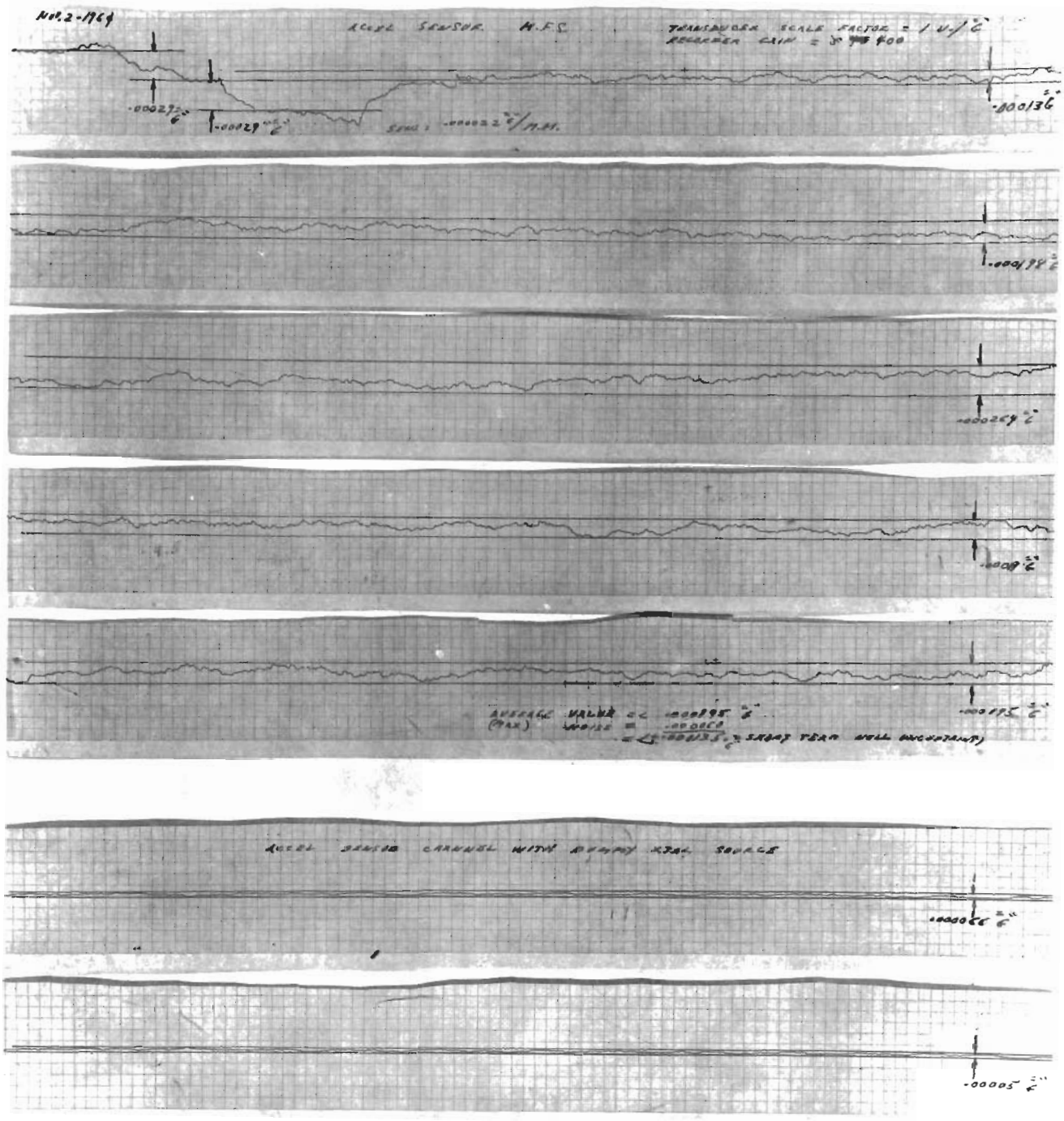

Figure 35. Recorded Test Data - Rate Sensor

4.2.1 Temperature Tests

The temperature test series was designed to separate the transducer borne errors from the electronic errors and was, to that end, divided into two test series.

4.2.1.1 Electronics Temperature Tests

The electronics elements tested included the isolation amplifier shown in Figure 36, the power supply shown in Figure 37, and a commercially available demodulator furnished by the Natal Engineering Corporation.

Because it was necessary to isolate the contributions of phase shift in the system, the isolation amplifier first was tested separately for its phase shift characteristics. The instrumentation setup included a phase sensitive voltmeter, with the input and output compared for phase shift with a standard 400 cps carrier with simulated loads and inputs, with only the isolation amplifier undergoing a thermal change. The uncompensated performance of the device is shown in Figure 38. It indicates a phase shift of no more than 0.6° from -65° to +200°F, which amounts to approximately ±.5% of full scale cross coupling error.

The next series of tests was run to determine the combination isolation amplifier and discriminator amplifier gain change over a temperature range with three discrete levels of input. These results are depicted in Figure 39. Indications are that for the range of -65° to +160°F, a total gain change of less than 1% occurred and operated in a linear fashion, that is, increasing gain with increasing temperature. This data combines all effects, including the reading error and the difference in scales from the high and low ranges on the instrumentation. While it was not intended to temperature test the electronics as the first emphasis, it was felt that some idea of their performance should be determined to insure that the order of magnitude of the various inputs were in balance. Thus, the demodulator null stability also was determined. These results are shown in Figure 40. While this demodulator circuit was not state-of-the-art, it was felt to be typical of commercially available devices.

4.2.1.2 Transducer Temperature Tests

As a first step in determining the transducer errors due to temperature, the permanent magnet excited two phase reference generator was tested for orthogonolity and phase shift under temperature. The instrumentation setup used the outputs of the generator's sine-cosine windings as the reference and signal, respectively, into a North Atlantic Phase Sensitive Volt Meter. The results of this test series is depicted in Figure 41, showing a phase shift of approximately 0.1° for the 200°F temperature band.

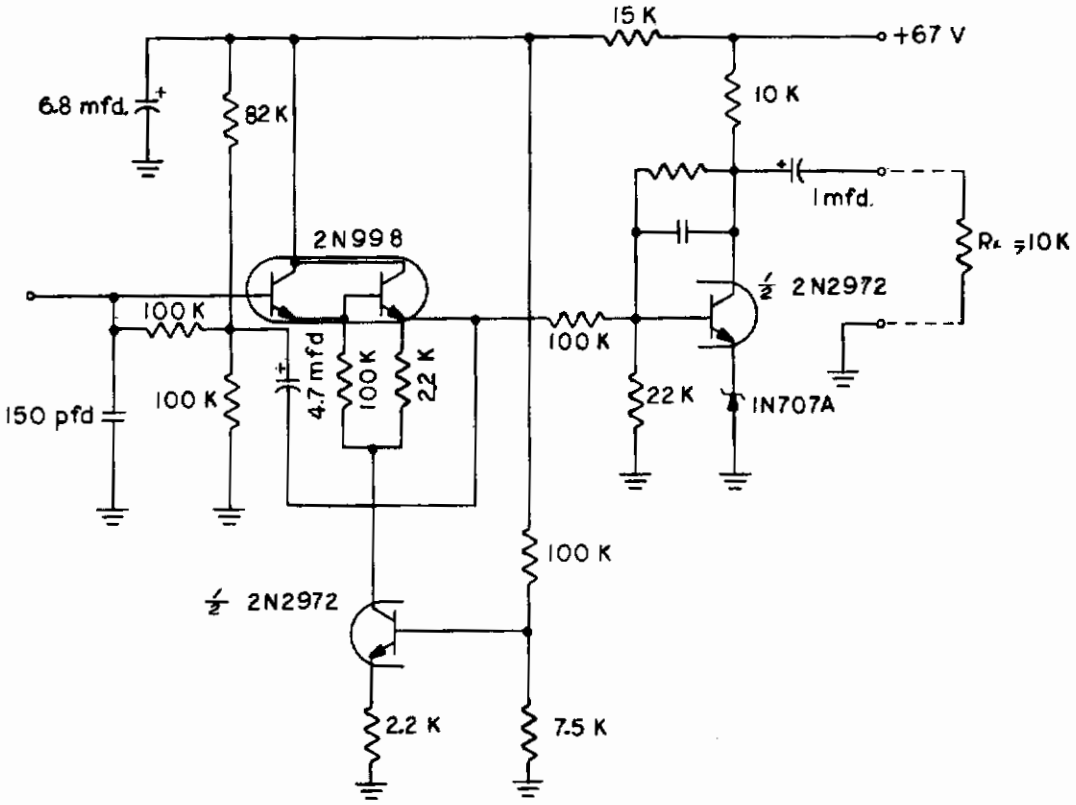

Figure 36. Isolation Amplifier Schematic

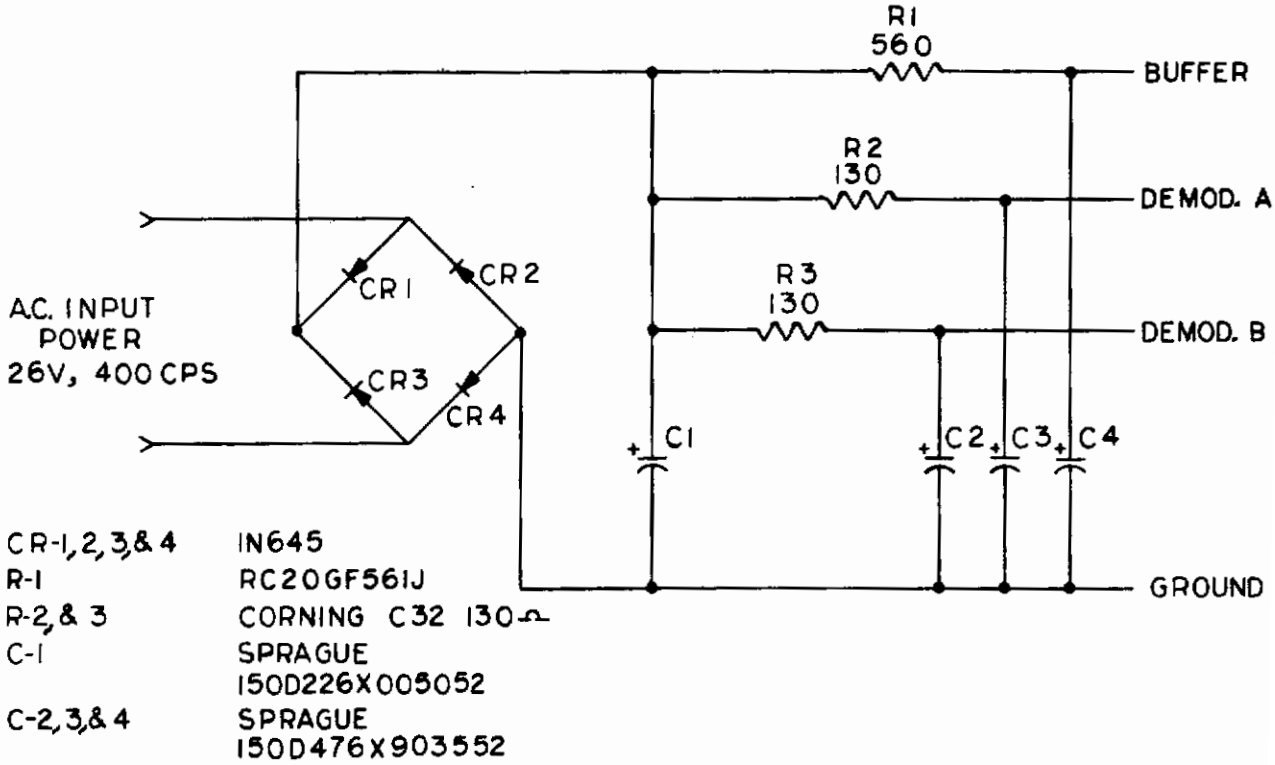

CR-1, 2, 3, & 4	IN645
R-1	RC20GF561J
R-2, & 3	CORNING C32 130Ω
C-1	SPRAGUE 150D226X005052
C-2, 3, & 4	SPRAGUE 150D476X903552

Figure 37. Isolation Amplifier and Demodulator Power Supply Schematic

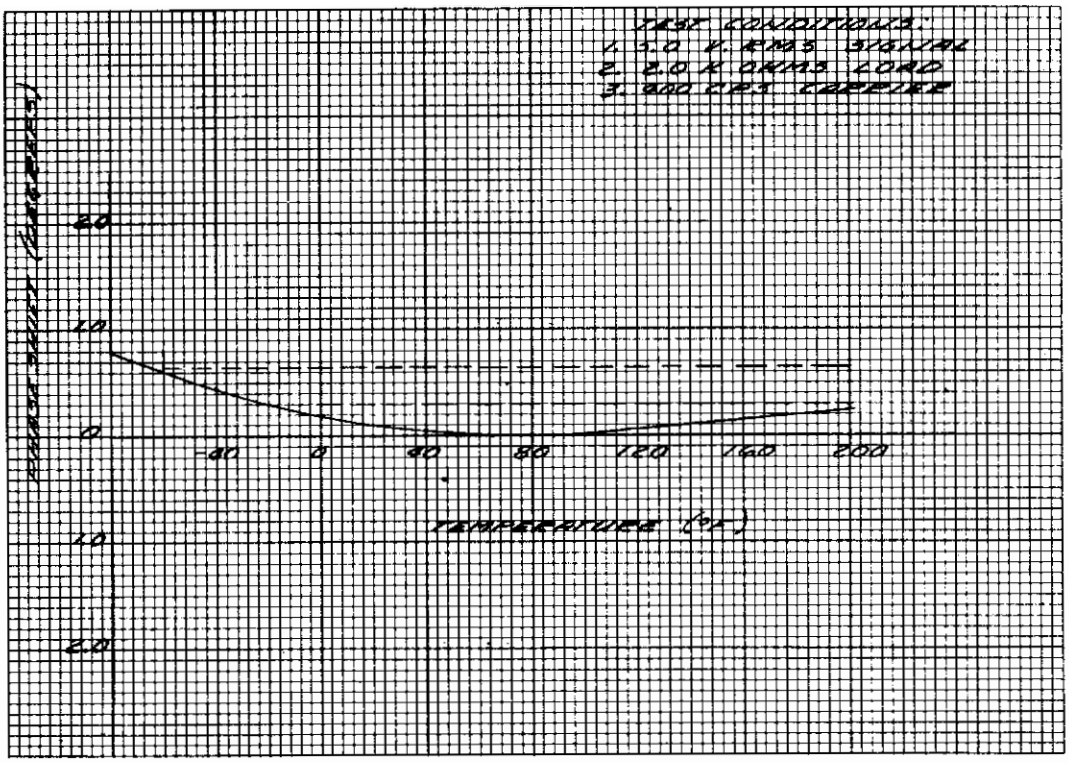

Figure 38. Isolation Amplifier Thermal Phase Shift Characteristics

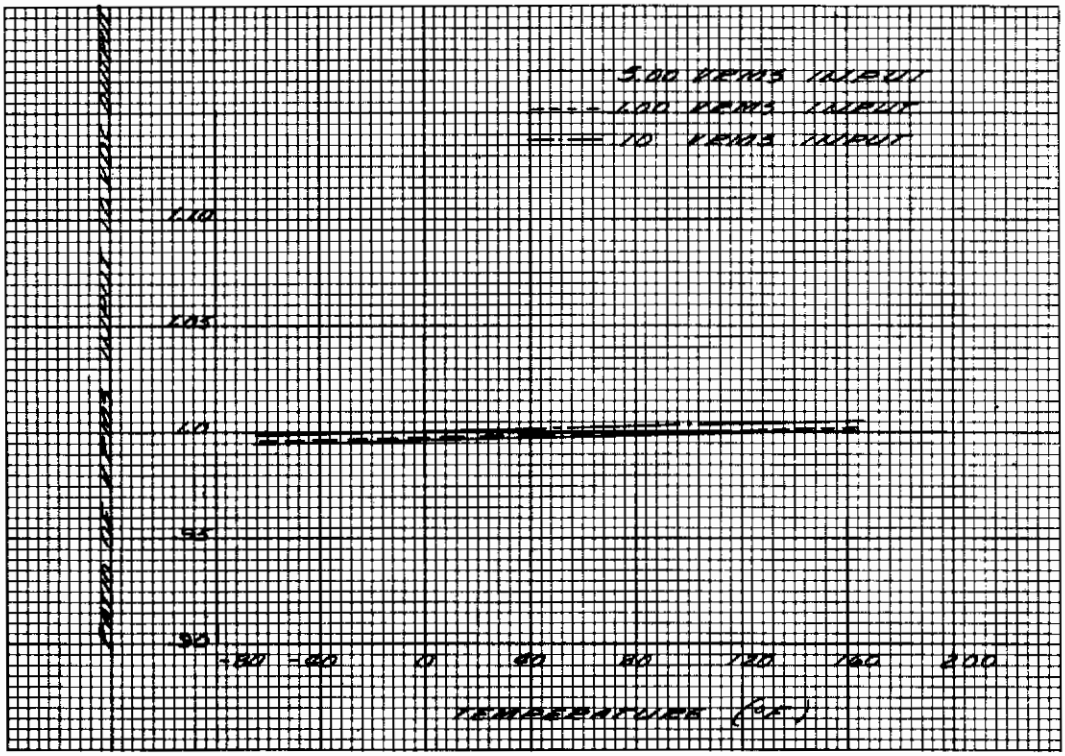

Figure 39. Combination Isolation Amplifier - Demodulator Thermal Gain Stability

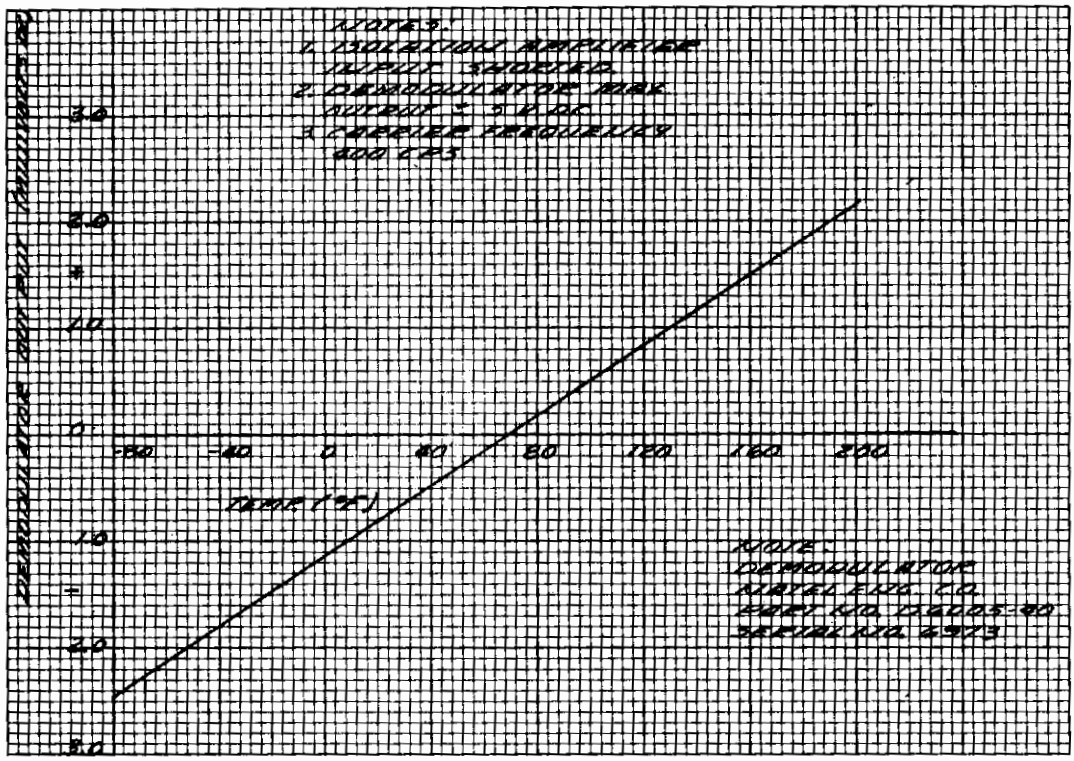

Figure 40. Demodulator Thermal Null Stability

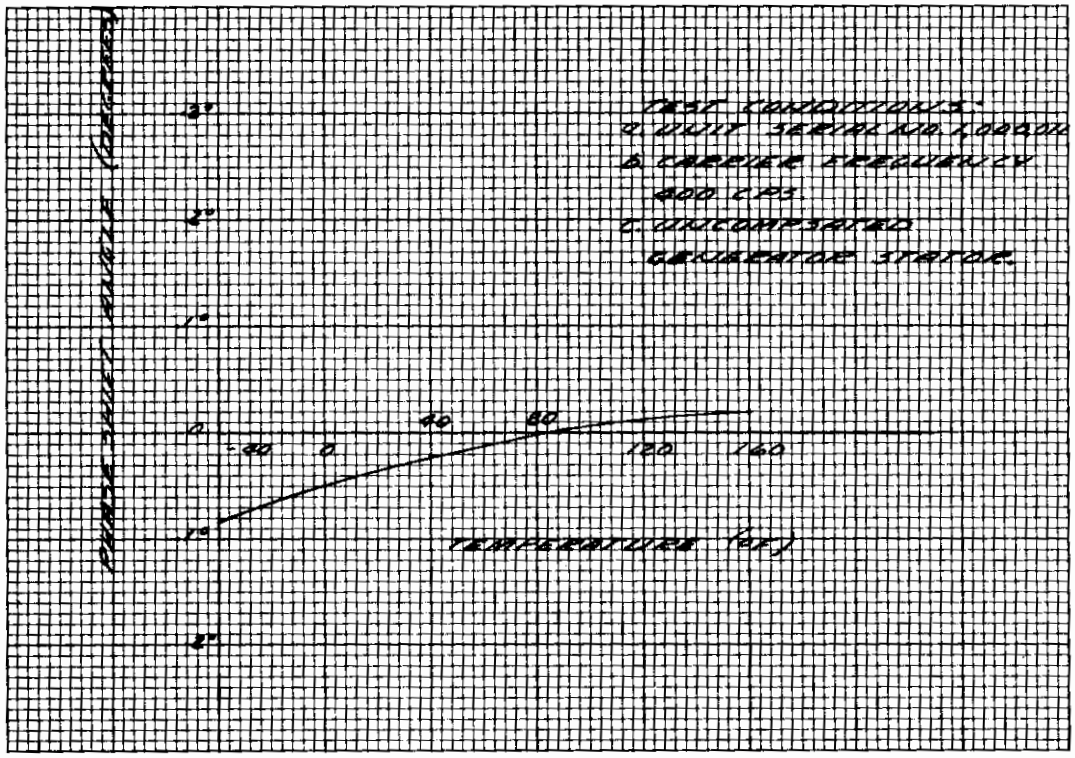

Figure 41. Reference Generator Thermal Phase Shift Characteristics

A series of tests were run on the rate sensing portion of the transducer from -40° to +160°F to determine output linearity and null uncertainty characteristics under temperature.

Figure 42 shows an output linearity of ±1.5% of full scale, and Figure 43 shows the null uncertainty from all effects, including the "G" sensitive term, to be within ±.03°/sec.

The next series of tests was for scale factor stability of the rate sensor and involved the unit mounted in an environmental chamber on the rate table. The isolation amplifier was placed immediately outside of the thermal environment, with provisions for adding a temperature compensation padding capacitor in parallel with the crystal at the isolation amplifier input. A series of tests was first made without the padding capacitor, up to and including the maximum input rate range, both clockwise and counterclockwise. An additional series of tests was run with a 200 uufd padding capacitor across the crystal output. It had been previously determined by the crystal material manufacturer that a nearly ideal temperature compensation existed for the crystal material in the form of a padding capacitor with a dielectric material of a negative temperature coefficient exhibiting a change of capacitance in the order of 750 ppm., per degree C. The results of this series, as shown in Figure 44, indicated that with a simple capacitor, selected on the basis of the desired sensitivity, compensation extending from -40° to +160°F was accomplished. This yielded an overall transducer temperature coefficient of approximately .01% per degree F. To determine that the scale factor change was linear at all operating input rate ranges, that is, with low, medium and high input rates, the linearity test series was run using the 200 uufd capacitor at the isolation amplifier input, bridging the crystal output. These test results also are shown in Figure 42.

4.2.2 Response Tests

4.2.2.1 Isolation Amplifier Response

In addition to the thermal phase shift test on the isolation amplifier, the frequency response characteristic was determined in the range of 100 to approximately 10,000 cps. The results of this series, as shown in Figure 45, indicate that for a 10% line frequency regulation, a 4% linear change in scale factor results.

4.2.2.2 Transducer Response Tests

The transducer was subjected to dynamic response testing for the rate sensor portion using the test fixture shown in Figures 46 and 47. This test series was run at 75°F ambient and consisted of the following elements: an angular oscillation drive capable of inputs from 1 to 150 cps at peak velocities of from 1°/sec. to 100°/sec. suitably mounted to an articulating mechanism for driving the rate sensor. The readout consisted of the resolved and discriminated rate sensor information which was applied to the vertical axis of an oscilliscope.

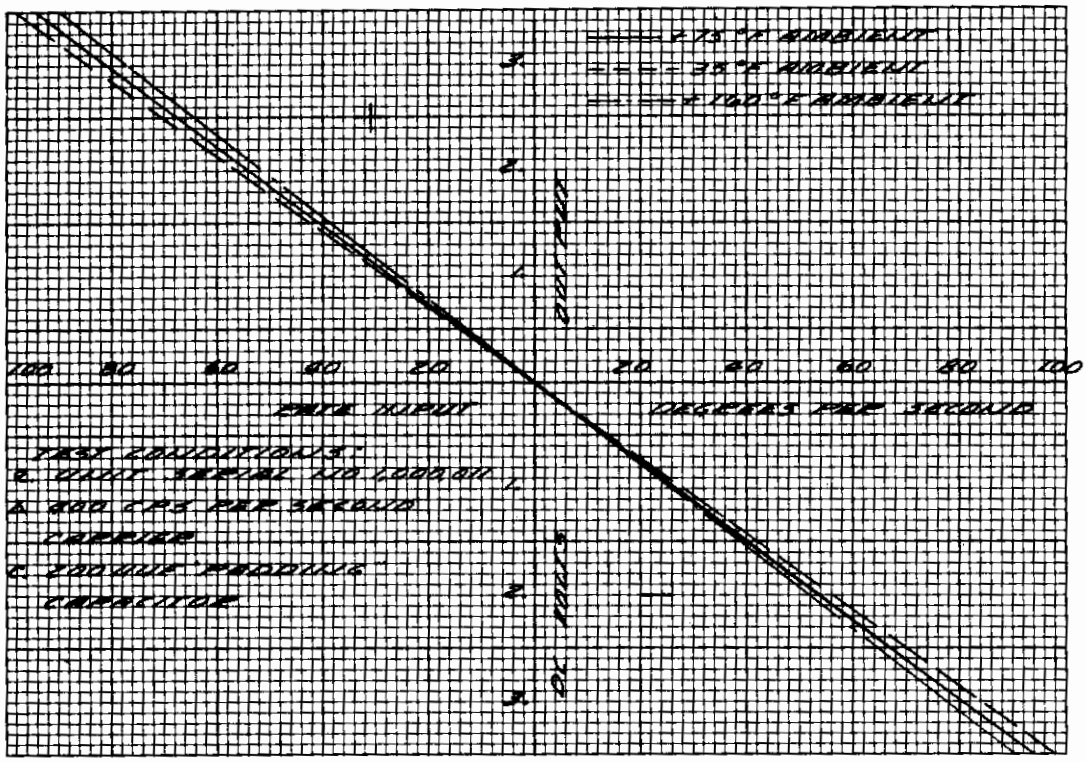

Figure 42. Rate Sensor Linearity Thermal Test Data

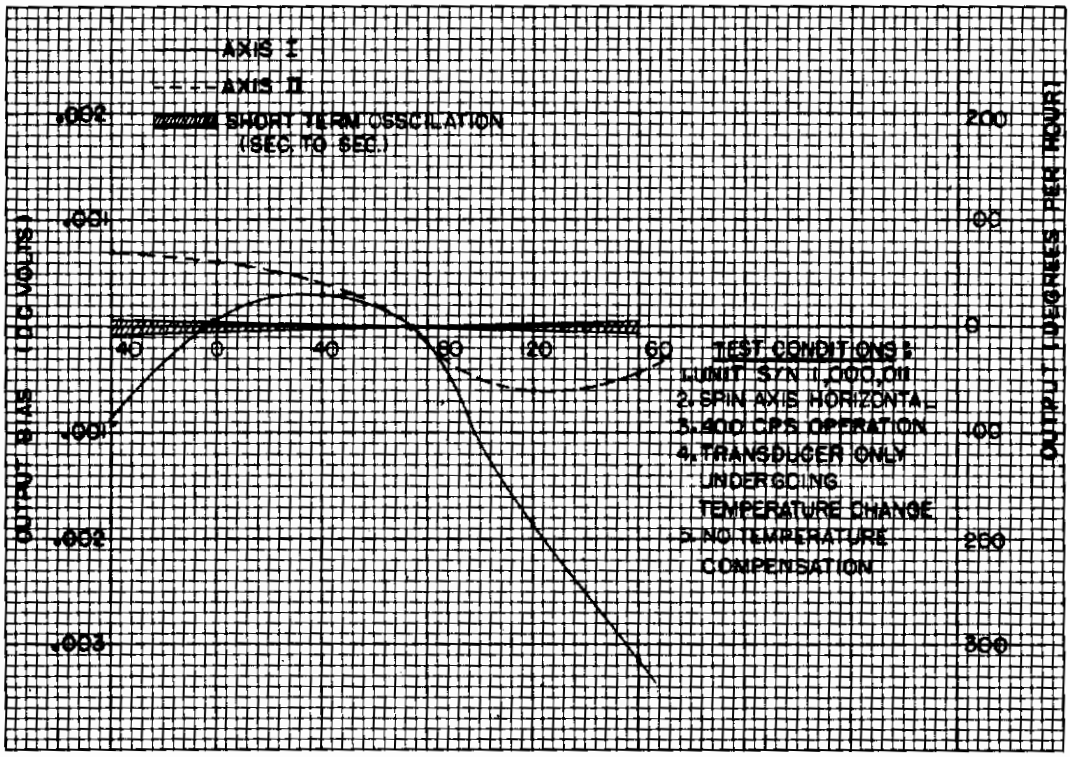

Figure 43. Rate Sensor Null Uncertainty Thermal Test Data

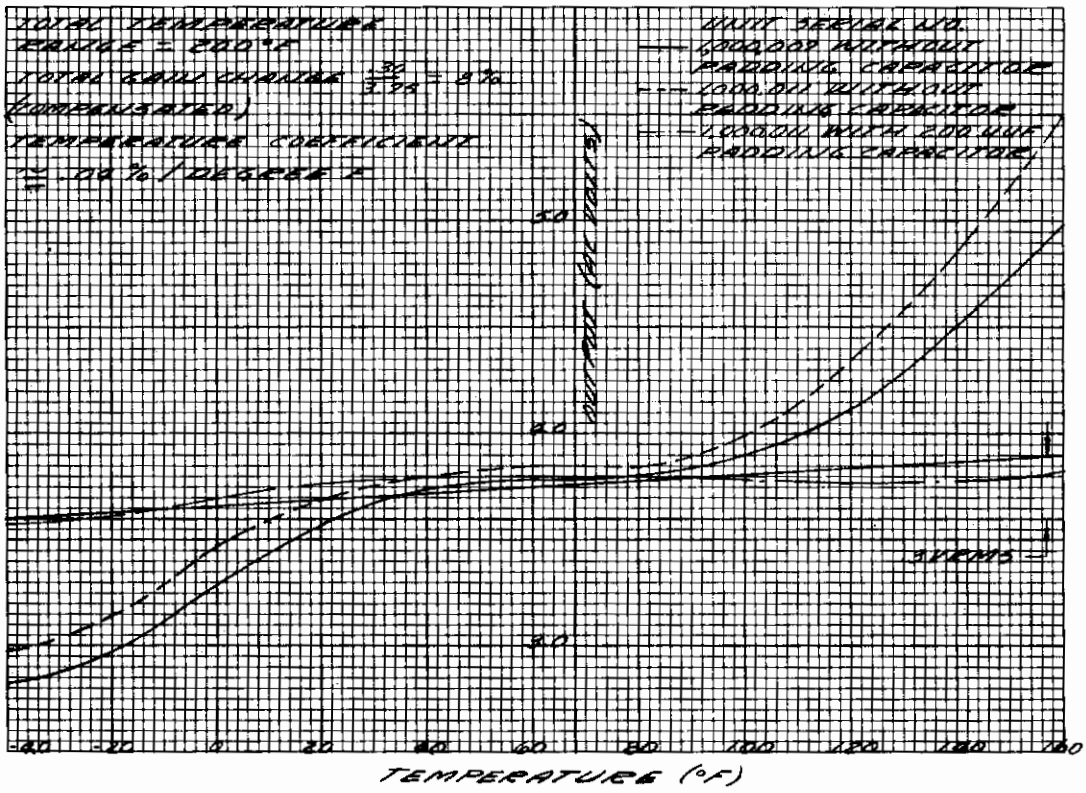

Figure 44. Rate Sensor Thermal Scale Factor Stability

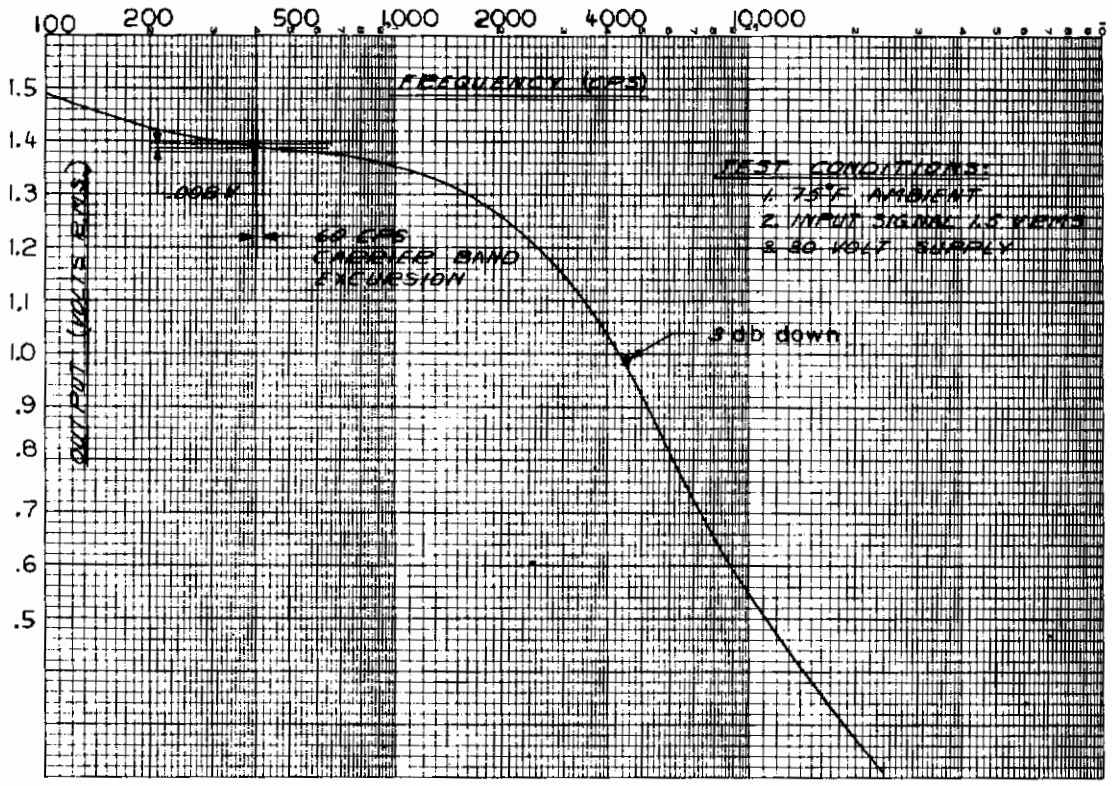

Figure 45. Isolation Amplifier Frequency Response

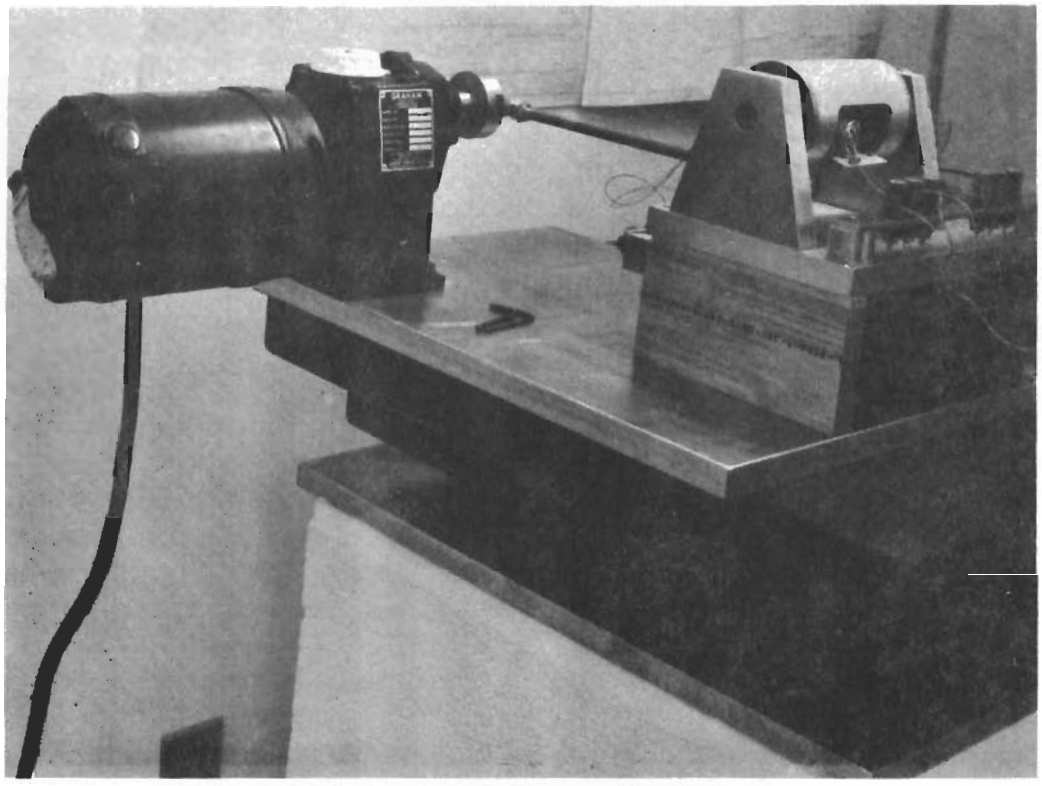

Figure 46. Angular Response Test Setup

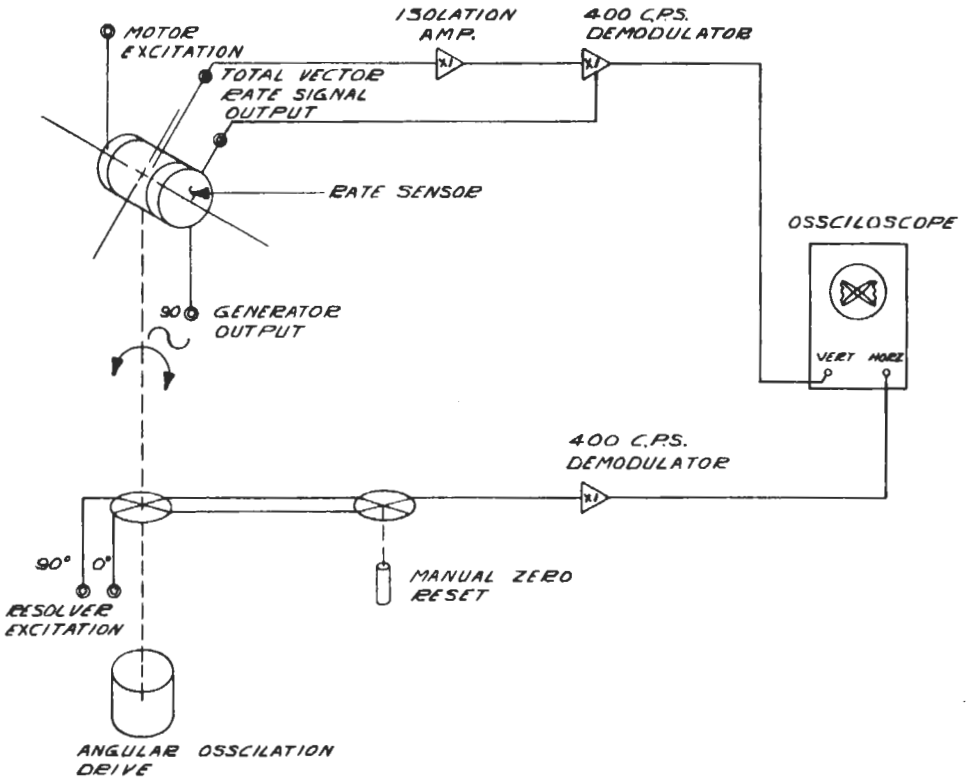

Figure 47. Angular Response Test Schematic

The reference signal to the oscilliscope horizontal axis was the resolved and demodulated angular position signal, derived from a resolver train and demodulator which was also mounted on the angular oscillation drive. With this readout setup exhibiting a lissajous presentation on the high persistance CRT, and with the capability for a manual zero reset in the angular position output of the table, direct phase information was obtained by "nulling" the resultant butterfly scope pattern at each discrete test frequency and amplitude.

In addition, with the use of the calibrated vertical amplitude control on the scope, a measurement of the amplitude of the rate sensor output was gained. The 400 cps demodulators used for the two outputs had an attenuation of 3 db at 80 cps and the data was compensated to take this into account. Figure 48 shows a typical plot for the rate sensor element in terms of amplitude and phase at frequencies of from 1 to 150 cps. The plot indicates a natural frequency of 75 to 85 cps and a damping ratio from .85 to 1.

4.3 PRELIMINARY SUMMARY OF PERFORMANCE TESTING

Based upon all the test data, the following observations can be made:

a) Reliable transducer outputs as low as 1 to 10 microvolts can be obtained.

b) Resolutions, scale factors, and dynamic null uncertainties are well within the 10^{-4} "G" and 1°/hr. class for the acceleration and angular rate elements, respectively. It is probable that both are 10 to 50 times better; however, instrumentation noise was the limiting factor.

c) With a maximum input of 500°/sec. in the rate sensor and 10 to 20 "G's" in the accelerometer, dynamic ranges in the order of one million to one can be obtained.

d) The accelerometer has no known major parameter deficiencies under steady-state environment. The rate sensor has one major and one minor one, i.e., the linear "G" sensitive term and the motor sync position effect, respectively.

e) Measurements of the inertial interaction between the two transducer outputs, that is, linear "G" errors in the rate sensor and angular velocity errors in the linear accelerometer, resulted in less than .02°/sec./"G" for the rate sensor and less than .001 "G"/deg/sec. for the accelerometer.

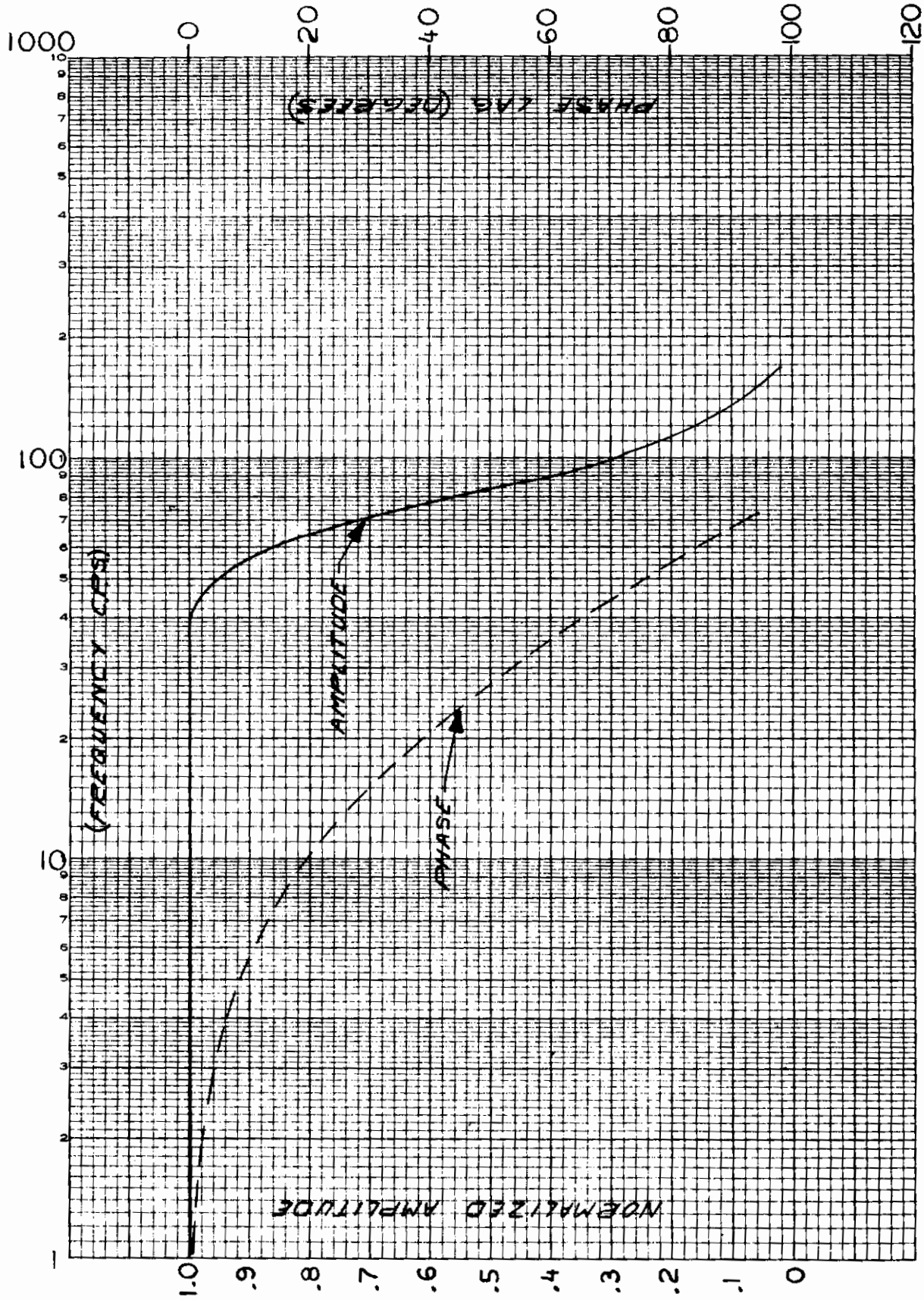

Figure 48. Angular Rate Sensor Dynamic Response

f) Linearities in both elements are known to be in the ±1% class, the ultimate precision was not determined because of the test equipment limitations.

g) A less than 3 to 1 change in the magnitude of bias, null uncertainty and "G" sensitive terms exists for a ±50°F temperature band.

5. CONCLUSIONS

The results of this program indicate the possibilities for an instrument with an enormous growth potential in terms of size reduction and performance improvement. Seen as real possibilities are highly advanced sensors packaged in an extremely small size, with modest power requirements, minimum readiness time and with a high order of reliability. The major characteristics clearly demonstrated during the program for this sensing technique include:

a) A transducer art which, either singly or in combination, can sense inertially derived information at "inertial" quality thresholds with dynamic ranges in excess of one million to one and at frequency responses of 100 to 1,000 cps.

b) A technique which, while already in the subminiature size class in the feasibility stage, clearly is capable of a size reduction in the order of ten to one in volume resulting in classes of devices in the "submicrominiature" class.

c) A technique with reliability indices improved 10 to 100 times when compared with contemporary rotating member gyros - the reliability index being based upon the results of a numerical parts comparison of this design concept with conventional subminiature rate gyros.

d) A concept leading directly to the possibilities for high order multiplexing, i.e., transducer types working in redundancy at the sensing level.

e) A technique where, because of its multiplex aspect and multimode output format, extremely flexible and very small inertial sensor packages, equally suitable for strapdown applications and gimbal stabilization modes, can be achieved.

The success of this research and development program investigating the feasibility of the multifunction technique can best be judged by comparing it with the design objectives which show that for an instrument somewhat below the size of the design objective, performance parameters were met or exceeded by a factor of 5 to 10; and, with the exception of power consumption, no operating characteristic goals were missed. (See Figure 49.) A column of values is also included in Figure 49 to emphasize the parameters of the multifunction sensor where "growth" can be predicted with continuing work in this area.

Further work in this inertial measuring technique should be directed at the utilization of some as yet undeveloped aspects of the concept such as geometric resolving and discriminating methods, geometric integration techniques and further major reductions in size and power consumption of the transducer with the use of integrated microelectronics.

MULTISENSOR TECHNIQUE INVESTIGATION

PARAMETERS	PROGRAM GOAL	ACHIEVED VALUES	PROJECTED GOALS
		Major Dia. 1.3 x .55" Length	Major Dia. .750" x 2" L.
Size	1" Dia. x 2.75"	Minor Dia. .8 x 2.5" Length	Minor Dia. .375" x 1.0" L.
Weight	<135 Gm's.	<115 Gm's.	<30 Gm's.
Power Consumption	<.6 Watts	7.6 V.A.	<2.5 V.A.
Activation Time	------	<2.7 Secs.	<1.5 Sec.
Temperature	-65 to +250°F	-65 to +250°F	-65 to +250°F
Shock	>50 "G"	>1500 "G"	>3000 "G"
Vibration	10 "G", 5 to 2000 cps	20 "G", 5 to 2000 cps	40 "G", 5 to 2000 cps
RATE SENSOR PERFORMANCE			
Threshold	<1°/hr.	<.5°/hr.	3.5°/hr.
Max. Rate	>200°/Sec.	>500°/Sec.	>1000°/Sec.
Scale Factor	.125V/Deg/Sec.	.075 V/Deg/Sec.	.025 V/Deg/Sec.
Frequency Response	75 cps	90 cps	>150 cps
Linearity	<1%	<1.25%	<1.25%
Damping Ratio	.5 to .7	.6 to .8	.6 to .8
Dynamic Range	720,000 to 1	3,600,000 to 1	1,000,000 to 1
Linear "G" Coupling	-------	<20°/hr/"G"	<1°/hr/"G"
ACCEL. SENSOR PERFORMANCE			
Threshold	$<10^{-4}$ "G"	$<10^{-5}$ "G"	$<10^{-4}$ "G"
Max. "G"	>40 "G"	>20 "G"	>50 "G"
Scale Factor	.5 V/"G"	1.0 V/"G"	.1 V/"G"
Frequency Response	150 cps	>3 kcps	>4 kcps
Linearity	<1%	<1%	<1%
Damping Ratio	.5 to .7	.5 to .7	.5 to .7
Dynamic Range	400,000 to 1	2,000,000 to 1	500,000 to 1
Angular Vel. Coupling	-------	<.001 "G"/Deg/Sec.	<.0001 "G"/Deg/Sec.

Figure 49

unclassified
Security Classification

DOCUMENT CONTROL DATA - R&D
(Security classification of title, body of abstract and indexing annotation must be entered when the overall report is classified)

1. ORIGINATING ACTIVITY (Corporate author)
Instrumentation & Control Operations, National Water Lift Company, Pneumo Dynamics Corporation, 3000 Kraft Avenue, SE, Grand Rapids, Michigan

2a. REPORT SECURITY CLASSIFICATION
unclassified

2b. GROUP

3. REPORT TITLE
MULTIFUNCTION SENSOR TECHNIQUE

4. DESCRIPTIVE NOTES (Type of report and inclusive dates)
Final Report

5. AUTHOR(S) (Last name, first name, initial)
Pittman, Roland (N.M.I.)

6. REPORT DATE	7a. TOTAL NO. OF PAGES	7b. NO. OF REFS
June 1965	58	none

8a. CONTRACT OR GRANT NO.	9a. ORIGINATOR'S REPORT NUMBER(S)
AF33(615)-1200 b. PROJECT NO. 8222 c. Task No. 822209 d.	9b. OTHER REPORT NO(S) (Any other numbers that may be assigned this report) AFFDL-TR-65-4

10. AVAILABILITY/LIMITATION NOTICES
Qualified requesters may obtain copies of this report from DDC.
Foreign announcement and dissemination of this report by DDC is not authorized.

11. SUPPLEMENTARY NOTES	12. SPONSORING MILITARY ACTIVITY
	Air Force Flight Dynamics Laboratory Research & Technology Division Wright-Patterson Air Force Base, Ohio

13. ABSTRACT

The applied research study, as described herein, relates to an investigation into the feasibility of a technique for sensing, simultaneously in two axes, angular velocity and linear acceleration in a transducer with one moving part.

Techniques for instrumenting inertial interactions in a rotating frame were employed, utilizing piezoelectric electrostrictive devices for instrumentation, and fluid bodies for the inertial reaction member and proof mass. The technique was reduced to practice, resulting in a subminiature, full integrated, compact, functional prototype wherein both types of outputs were provided in each of two orthogonal sensing axes. An integrated prototype was evaluated for all major performance parameters and operational characteristics.

The results have revealed a transducer technique capable of angular velocity sensing thresholds of 1°/hr. and linear acceleration sensing thresholds of 10^{-5} "G", with dynamic ranges in each of the two quantities in excess of one million to one. Also demonstrated, within the study, was the potential for high reliability redundant sensing techniques and further size and power consumption reduction while maintaining the extreme sensing thresholds.

DD FORM 1 JAN 64 1473

unclassified
Security Classification

14. KEY WORDS	LINK A		LINK B		LINK C	
	ROLE	WT	ROLE	WT	ROLE	WT
Multifunction Sensor Two-Axis Inertial Sensor Fluid Rotor Angular Rate Sensor Linear Accelerometer DART (Dual Axis Rate Transducer) Hydrodynamic Gas Bearing						

INSTRUCTIONS

1. ORIGINATING ACTIVITY: Enter the name and address of the contractor, subcontractor, grantee, Department of Defense activity or other organization *(corporate author)* issuing the report.

2a. REPORT SECURITY CLASSIFICATION: Enter the overall security classification of the report. Indicate whether "Restricted Data" is included. Marking is to be in accordance with appropriate security regulations.

2b. GROUP: Automatic downgrading is specified in DoD Directive 5200.10 and Armed Forces Industrial Manual. Enter the group number. Also, when applicable, show that optional markings have been used for Group 3 and Group 4 as authorized.

3. REPORT TITLE: Enter the complete report title in all capital letters. Titles in all cases should be unclassified. If a meaningful title cannot be selected without classification, show title classification in all capitals in parenthesis immediately following the title.

4. DESCRIPTIVE NOTES: If appropriate, enter the type of report, e.g., interim, progress, summary, annual, or final. Give the inclusive dates when a specific reporting period is covered.

5. AUTHOR(S): Enter the name(s) of author(s) as shown on or in the report. Enter last name, first name, middle initial. If military, show rank and branch of service. The name of the principal author is an absolute minimum requirement.

6. REPORT DATE: Enter the date of the report as day, month, year; or month, year. If more than one date appears on the report, use date of publication.

7a. TOTAL NUMBER OF PAGES: The total page count should follow normal pagination procedures, i.e., enter the number of pages containing information.

7b. NUMBER OF REFERENCES: Enter the total number of references cited in the report.

8a. CONTRACT OR GRANT NUMBER: If appropriate, enter the applicable number of the contract or grant under which the report was written.

8b, 8c, & 8d. PROJECT NUMBER: Enter the appropriate military department identification, such as project number, subproject number, system numbers, task number, etc.

9a. ORIGINATOR'S REPORT NUMBER(S): Enter the official report number by which the document will be identified and controlled by the originating activity. This number must be unique to this report.

9b. OTHER REPORT NUMBER(S): If the report has been assigned any other report numbers *(either by the originator or by the sponsor)*, also enter this number(s).

10. AVAILABILITY/LIMITATION NOTICES: Enter any limitations on further dissemination of the report, other than those imposed by security classification, using standard statements such as:

(1) "Qualified requesters may obtain copies of this report from DDC."

(2) "Foreign announcement and dissemination of this report by DDC is not authorized."

(3) "U. S. Government agencies may obtain copies of this report directly from DDC. Other qualified DDC users shall request through _____."

(4) "U. S. military agencies may obtain copies of this report directly from DDC. Other qualified users shall request through _____."

(5) "All distribution of this report is controlled. Qualified DDC users shall request through _____."

If the report has been furnished to the Office of Technical Services, Department of Commerce, for sale to the public, indicate this fact and enter the price, if known.

11. SUPPLEMENTARY NOTES: Use for additional explanatory notes.

12. SPONSORING MILITARY ACTIVITY: Enter the name of the departmental project office or laboratory sponsoring *(paying for)* the research and development. Include address.

13. ABSTRACT: Enter an abstract giving a brief and factual summary of the document indicative of the report, even though it may also appear elsewhere in the body of the technical report. If additional space is required, a continuation sheet shall be attached.

It is highly desirable that the abstract of classified reports be unclassified. Each paragraph of the abstract shall end with an indication of the military security classification of the information in the paragraph, represented as *(TS), (S), (C), or (U)*.

There is no limitation on the length of the abstract. However, the suggested length is from 150 to 225 words.

14. KEY WORDS: Key words are technically meaningful terms or short phrases that characterize a report and may be used as index entries for cataloging the report. Key words must be selected so that no security classification is required. Identifiers, such as equipment model designation, trade name, military project code name, geographic location, may be used as key words but will be followed by an indication of technical context. The assignment of links, rules, and weights is optional.